Article

Cell Reports

Neuropilin-1 Is Expressed on Lymphoid Tissue Residing LTi-like Group 3 Innate Lymphoid Cells and Associated with Ectopic Lymphoid Aggregates

Graphical Abstract

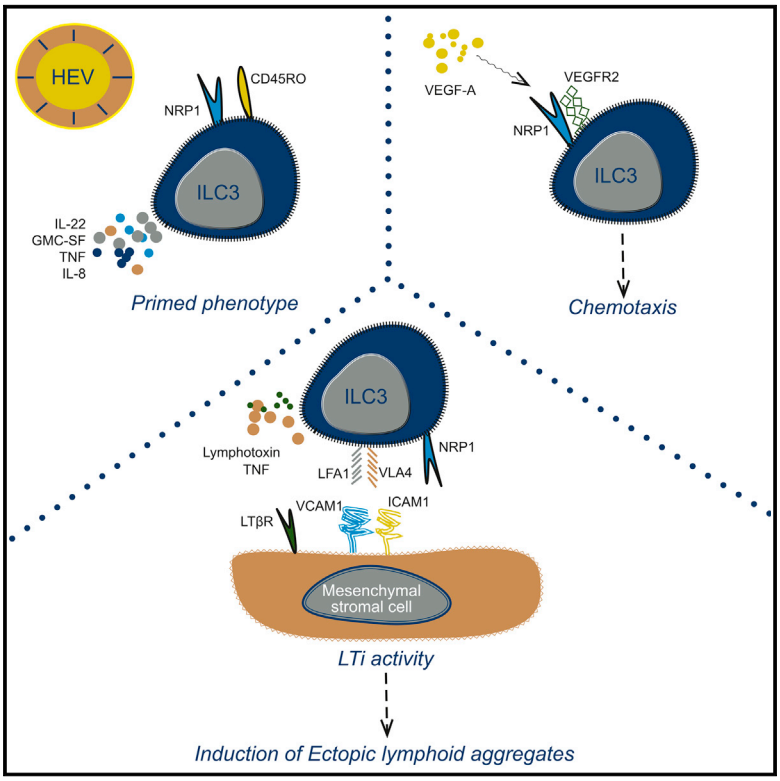

Highlights

- NRP1$^+$ ILC3s are present in lymphoid tissues, but not in the peripheral blood or skin
- NRP1$^+$ ILC3s express CD45RO and produce higher amounts of cytokines than NRP1$^-$ ILC3s
- NRP1 is a marker for human ILC3s with LTi phenotype and in vitro LTi activity
- NRP1$^+$ ILC3s are present in lung tissues from smokers and COPD patients

Authors

Medya Mara Shikhagaie, Åsa K. Björklund, Jenny Mjösberg, ..., Melanie Bruchard, Bianca Blom, Hergen Spits

Correspondence

m.m.shikhagaie@amc.uva.nl (M.M.S.), hergen.spits@amc.uva.nl (H.S.)

In Brief

Shikhagaie et al. find that NRP1 expressing human ILC3s are LTi-like cells, which are present in fetal tissues and adult lymphoid tissues, but not in peripheral blood or skin. NRP1$^+$ ILC3s cells are primed and migrate in response to VEGF-A. In addition, their presence in the lungs of smokers and COPD patients provides insight into the formation of ectopic lymphoid aggregates.

Shikhagaie et al., 2017, Cell Reports *18*, 1761–1773
February 14, 2017
http://dx.doi.org/10.1016/j.celrep.2017.01.063

Cell Reports
Article

Neuropilin-1 Is Expressed on Lymphoid Tissue Residing LTi-like Group 3 Innate Lymphoid Cells and Associated with Ectopic Lymphoid Aggregates

Medya Mara Shikhagaie,[1,7,*] Åsa K. Björklund,[2] Jenny Mjösberg,[3] Jonas S. Erjefält,[4] Anne S. Cornelissen,[5] Xavier Romero Ros,[1] Suzanne M. Bal,[1] Jasper J. Koning,[6] Reina E. Mebius,[6] Michiko Mori,[4] Melanie Bruchard,[1] Bianca Blom,[1] and Hergen Spits[1,*]

[1]Department of Experimental Medicine, Academic Medical Center, University of Amsterdam, 1105 AZ Amsterdam, the Netherlands
[2]Department of Cell and Molecular Biology, Karolinska Institutet, 171 77 Stockholm, Sweden
[3]Center for Infectious Medicine, Department of Medicine Huddinge, Karolinska Institutet, 171 77 Stockholm, Sweden
[4]Unit of Airway Inflammation, Department of Experimental Medical Sciences, Lund University, 221 84 Lund, Sweden
[5]Department of Hematopoiesis, Sanquin Research and Landsteiner Laboratory, Academic Medical Center, University of Amsterdam, 1006 AN Amsterdam, the Netherlands
[6]Department of Molecular Cell Biology and Immunology, VU University Medical Center, 1081 HV Amsterdam, the Netherlands
[7]Lead Contact
*Correspondence: m.m.shikhagaie@amc.uva.nl (M.M.S.), hergen.spits@amc.uva.nl (H.S.)
http://dx.doi.org/10.1016/j.celrep.2017.01.063

SUMMARY

Here, we characterize a subset of ILC3s that express Neuropilin1 (NRP1) and are present in lymphoid tissues, but not in the peripheral blood or skin. NRP1$^+$ group 3 innate lymphoid cells (ILC3s) display in vitro lymphoid tissue inducer (LTi) activity. In agreement with this, NRP1$^+$ ILC3s are mainly located in proximity to high endothelial venules (HEVs) and express cell surface molecules involved in lymphocyte migration in secondary lymphoid tissues via HEVs. NRP1 was also expressed on mouse fetal LTi cells, indicating that NRP1 is a conserved marker for LTi cells. Human NRP1$^+$ ILC3s are primed cells because they express CD45RO and produce higher amounts of cytokines than NRP1$^-$ cells, which express CD45RA. The NRP1 ligand vascular endothelial growth factor A (VEGF-A) served as a chemotactic factor for NRP1$^+$ ILC3s. NRP1$^+$ ILC3s are present in lung tissues from smokers and patients with chronic obstructive pulmonary disease, suggesting a role in angiogenesis and/or the initiation of ectopic pulmonary lymphoid aggregates.

INTRODUCTION

Innate lymphoid cells (ILCs) can be divided into three groups based on distinct cytokine secretion profiles and the transcription factors they depend on. Group 3 ILCs (ILC3s), which are dependent on the transcription factor retinoic acid-related orphan receptor-gamma t (RORγt), encompass the related lymphoid tissue inducer (LTi) cells and ILC3 subsets (Artis and Spits, 2015). LTi cells promote lymphoid organogenesis and postnatal mucosal immunity through activation of stromal cells via lymphotoxin and tumor necrosis factor (TNF) (Cupedo et al., 2009). ILC3s produce interleukin (IL)-22, granulocyte-macrophage colony-stimulating factor (GM-CSF), TNF-α, IL-17A, B-cell activating factor (BAFF), and IL-8 in a stimulus-dependent manner and can promote tissue remodeling, wound healing, tolerance, anti-bacterial immunity, or chronic inflammation (Mjösberg and Spits, 2016). ILC3s exhibit distinctive phenotypes in different tissues, reflecting different stages of differentiation or activation. Recently, single-cell RNA sequencing (scRNA-seq) data from non-inflamed human tonsil found three ILC3 subpopulations, namely NKp44$^+$ ILC3s, CD62L$^+$ ILC3s, and human leukocyte antigen (HLA)-DR$^+$ ILC3s (Björklund et al., 2016).

ILC3s and LTi cells are closely related; however, in the mouse, these cells develop via distinct pathways (Killig et al., 2014). Whether this is also the case in humans is unknown, partly because of the lack of known markers for human LTi cells. Chemokine receptors (CCR)6, which in the mouse is selectively expressed in LTi-like cells, is expressed on almost all ILC3s in humans (Roan et al., 2016) and is therefore not a useful marker for human LTi cells. Recently, LTi-like cells in adult mice were described to express transcripts for Neuropilin 1 (NRP1) (Robinette et al., 2015). It was not determined whether mouse fetal LTi cells that are essential for the formation of secondary lymphoid organs express NRP1.

In this study, we investigated expression of Neuropilin 1 (NRP1, also called CD304, BDCA4) on human ILC3s. NRP1 was originally identified as a neural adhesion molecule that functions during the development of the embryonic nervous system and vascularization, but recent studies have demonstrated that NRP1 plays also a role in the immune system. NRP1 is able to interact with multiple ligands, such as secreted class 3 semaphorins, vascular endothelial growth factor A (VEGF-A) and transforming growth factor (TGF)-β1. NRP1 has

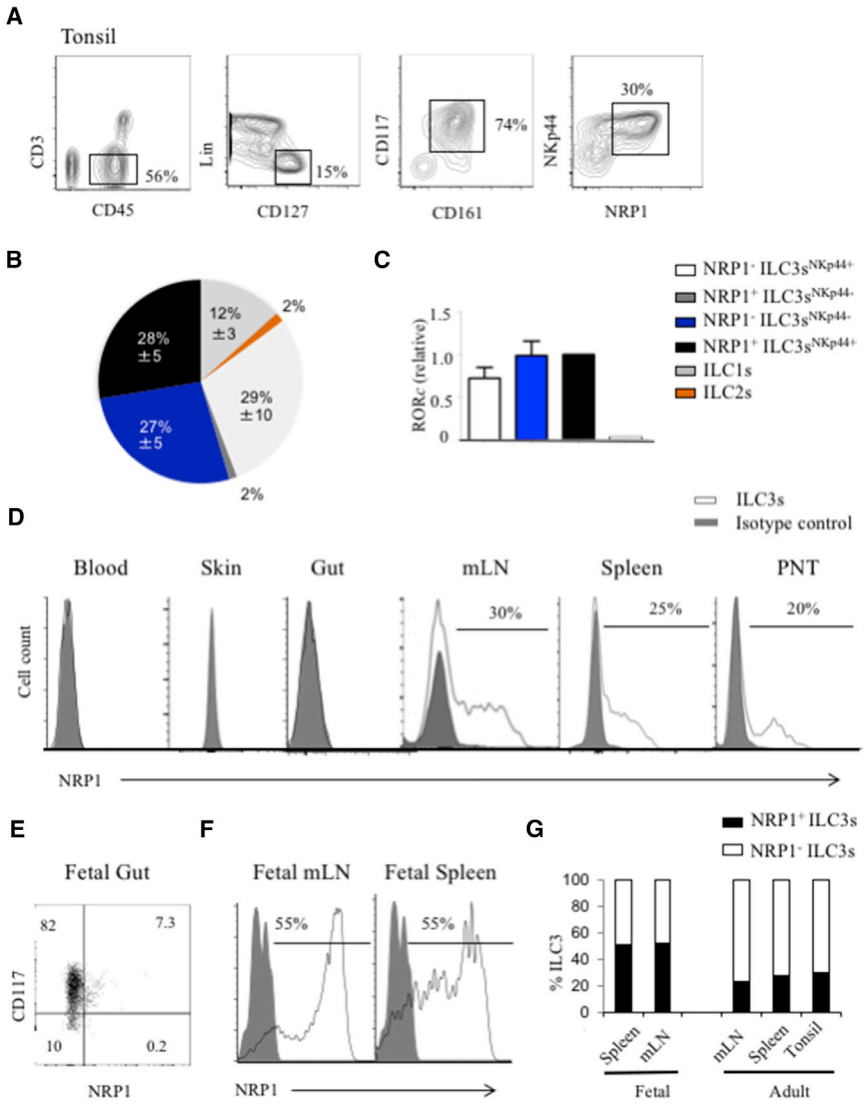

Figure 1. NRP1$^+$ ILC3s Are Present in Lymphoid Tissues but Not in the Peripheral Blood or Skin

(A) Flow cytometry analysis of human tonsil cell suspension; representative dot plots of gating strategy lineage CD3$^-$CD45$^+$CD127$^+$CD161$^+$CD117$^+$ ILC3s. Lineage mixture of antibodies added to exclude leukocytes includes CD3, TCRα/β, TCRγ/δ (T cells), CD14 (monocytes), CD16 (monocytes, NK cells), CD19 (B cells), CD94 (NK cells), FcεR1α (mast cell) and CD123, and BDCA2 (pDCs).

(B) Pie diagram showing mean frequency of ILC2s, ILC1s, and ILC3$^{NKp44+/-NRP1+/-}$ in human tonsil.

(C) Transcriptional analysis using qRT-PCR showing the relative expression of *RORγt* in tonsillar NRP1$^+$ ILC3s, NRP1$^-$ ILC3s, NRP1$^-$ NKp44$^-$ ILC3, and ILC1. Samples were normalized to mRNA encoding β-actin (*ACTB*). Data are representative of three independent experiments and donors.

(D) Expression of NRP1 analyzed by flow cytometry, on ILC from adult lymphoid and non-lymphoid tissue, including peripheral blood, skin, gut, mLN, spleen, and post-natal thymus. Filled histogram shows isotype control.

(E) Dot plot representing the expression of NRP1 and CD117 on ILCs from fetal gut, analyzed by flow cytometry.

(F) Expression of NRP1 (open histogram) analyzed by flow cytometry, on ILC3s from fetal mLN and fetal spleen. Filled histogram shows isotype control.

(G) Percentage of NRP1$^+$ (black bar) and NRP1$^-$ (white bar) ILC3s in fetal and adult lymphoid tissue. Data are mean of three to four donors.

a short cytoplasmic domain that lacks signaling activity, but together with the co-receptor vascular endothelial growth factor receptor 2 (VEGFR2) it forms a high-affinity complex for several isoforms of VEGF-A, which has potent proinflammatory properties, including an ability to mediate leukocyte trafficking into sites of inflammation (Edelbauer et al., 2010). NRP1 is expressed on various immune cell types including human plasmacytoid dendritic cells (pDCs), naive T cells, and a subset of CD4$^+$ T follicular helper cells in secondary lymphoid organs. NRP1 is also expressed by human T regulatory (Treg) cells present in secondary lymphoid organs, but not by Treg cells in peripheral blood (Milpied et al., 2011). In mice, NRP1 is selectively expressed by thymus-derived murine Treg cells, but not by in-vivo- or in-vitro-generated peripheral Treg cells (Yadav et al., 2012).

Here we report that NRP1 is expressed on a subset of human group 3 ILCs, which are present in lymphoid tissues and have in vitro LTi cell activity. We also observed that NRP1$^+$ ILC3s express CD45RO, whereas most NRP1$^-$ ILC3s expressed CD45RA, and that NRP1$^+$ cells produced higher levels of cytokines than NRP1$^-$ ILC3s upon in vitro cell activation. NRP1 was found to be associated with VEGFR2 on ILC3s and VEGF-A-induced migration of these cells in vitro. Taken together, our data indicate that NRP1 is functionally expressed on primed LTi cells in humans.

RESULTS

Human NRP1$^+$ ILC3s Are Only Present in Lymphoid Tissues

Flow cytometric analysis of tonsillar ILCs revealed that a subset of ILC3s express NRP1 (Figure 1A). NRP1 expression was mainly detected on NKp44 (Figure 1A) and CD56$^+$ ILC3s in the tonsil, whereas ILC1 (CD117$^-$NKp44$^-$) and ILC2 (CD117$^{-/+}$NKp44$^-$CRTH2$^+$) subsets lacked the expression of NRP1 (data not shown). NRP1$^+$NKp44$^+$ ILC3s represented approximately 28% (SD ± 5) of the total ILC population in the tonsil, and approximately 2% (SD ±1%) of NRP1$^+$ ILC3s were NKp44-negative (Figure 1B). The gene expression profile of analyzed ILC3s by qRT-PCR showed that all CD117$^+$ ILC3s, including the NRP1$^-$ and NRP1$^+$ ILC3s, express the ILC3

signature transcription factor *RORγt* (Figure 1C). Previous data indicate that these CD117$^+$CRTH2$^-$ ILC3s also express RORγt protein (Scoville et al., 2016; Bernink et al., 2015).

We examined the expression of NRP1 on ILCs in different lymphoid and non-lymphoid tissues. NRP1 expression was selectively expressed on ILC3s and limited to lymphoid tissues including mesenteric lymph node (mLN), post-natal thymus, spleen, and tonsil. Approximately 30% (SD ±5%) of ILC3s in the adult spleen and mLN expressed NRP1 (Figure 1D). NRP1$^+$ ILC3s were not present in the peripheral blood (Figure 1D), cord blood (data not shown), and skin (Figure 1D). They were also absent in the gut of patients with Crohn's disease, whereas these cells were present in the mLN of the same patient (Figure 1D).

We next compared lymphoid tissue NRP1$^+$ ILC3s with their fetal counterparts. We detected NRP1$^+$ ILC3s in the fetal liver, gut, mLN, and spleen. We observed a higher frequency (SD 50% ± 5% of total ILC3) of NRP1$^+$ ILC3s in fetal tissues compared with tonsils and adult mLN and spleen (Figures 1E and 1F). We also detected NRP1 on a small population of fetal gut ILC3s (SD 6.5% ± 1% of total ILC3s) (Figure 1E). We next assessed a set of surface proteins on NRP1$^-$ and NRP1$^+$ ILC3s by flow cytometry and compared these findings with published single-cell RNA sequencing (scRNA-seq) data generated from freshly isolated tonsil ILC subsets (Björklund et al., 2016). This analysis confirmed that tonsillar ILC3s (NKp44$^{+/-}$) express *RORc* and *NRP1*. Similar to NRP1 protein, *NRP1* was only expressed on ILC3s, whereas NK cells and ILC1 and ILC2 subsets lacked the expression of *NRP1*. In addition, NKp44/*NCR2*, PD1/*PDCD1*, and to a lesser extent NKp30/*NCR3* and CD2/*CD2* were expressed higher in NRP1$^+$ ILC3s at both protein and mRNA levels (Figure S1A). HLA-DR, RANKL, and inducible T-cell costimulator (ICOS) proteins were similarly expressed by NRP1$^+$ and NRP1$^-$ ILC3s, whereas expression of mRNAs encoding these molecules were slightly different in NRP1$^+$ compared with NRP1$^-$ ILC3s (Figure S1A). NRP1$^+$ ILC3s in the tonsil expressed higher levels of CCR6 and C-X-C chemokine receptor 5 (CXCR5) (Figure S1A). Fetal mLN and splenic ILC3s were mostly negative for NKp44, and the few NKp44$^+$ ILC3s contained similar proportions of NRP1$^+$ and NRP1$^-$ cells, indicating that the expression of NRP1 and NKp44 are not co-regulated in fetal tissues (Figure S2B). NRP1$^+$ ILC3s had similar levels of CCR6 and CXCR5 and lower CD161 expression compared with NRP1$^-$ ILC3s in fetal mLN (Figure S1B).

Single-Cell Transcriptomes of *NRP1*-Positive and *NRP1*-Negative ILC3 Populations

We used scRNA-seq data (Björklund et al., 2016) to further assess the expression of a selected set of genes typically expressed by ILC3s. Transcripts for many transcription factors, cytokines, and cytokine receptors including *AHR*, *TOX*, *TOX2*, *IL-23R*, *IL-1R1*, *CSF2*, *LTα*, and *LTβ*, showed higher expression in *NRP1*$^+$ compared with *NRP1*$^-$ ILC3s (Figure 2A). These data indicate that *NRP1*$^+$ ILC3 may be more mature and/or activated as compared with *NRP1*$^-$ ILC3s.To get a more unbiased functional characterization of *NRP1*$^+$ ILC3s, we assessed genes that shared direction with *NRP1* in a principal component analysis (PCA) of the ILC3s transcriptomes. The negative principal component 2 (PC2) included *NRP1* as well as several ILC3-specific markers. Those genes were subjected to a gene set enrichment test using Gene Ontology (GO) annotations (Reference Genome Group of the Gene Ontology Consortium, 2009) and using curated gene sets from Molecular Signatures Database (MSigDB) (Subramanian et al., 2005). The top gene sets that were enriched were GO term "Cell chemotaxis" (Figure 2B) and Reactome pathways "Chemokine receptors bind chemokines" and "Immunoregulatory interaction between a lymphoid and non-lymphoid cell" (Figure 2C) (adjusted p values are 4.0×10^{-5}, 8.1×10^{-4}, and 8.6×10^{-5}, respectively).

Genes in the chemokine receptor-chemokine binding gene set included the chemokine receptors *CXCR5*, *CCL20*, *CCR6*, and *CCR7* (Figure 2D). The expression for *CXCR5*, *CCL20*, and *CCR6* were higher and *CCR7* expression was lower in the *NRP1*$^+$ ILC3s compared with *NRP1*$^-$ ILC3s. These chemokine receptors determine selective migration in response to chemotactic stimuli, e.g., the chemokine (C-X-C motif) ligand 13 (CXCL13) and its receptor CXCR5 are involved in the homing of lymphocytes to lymph node follicles. The expression of the T lymphocyte (and ILC) recruiting factor chemokine ligand (CCL) 20 (macrophage inflammatory protein-3 alpha [MIP-3α]) suggests that *NRP1*$^+$ ILC3s, besides expressing high levels of CCR6, also may have the capacity to position CCR6$^+$ lymphocytes to or within lymphoid tissues. These results indicate that *NRP1*/NRP1 may be involved in the retention of ILC3s in lymphoid tissue. Genes enriched within the "Immunoregulatory interaction between a lymphoid and non-lymphoid cell" pathway included the integrin *ITGB1* (encoding CD29, integrin β1, receptor for vascular cell adhesion molecule [VCAM]1), class I MHC-restricted T cell-associated molecule (encoding CRTAM, CD355), *SELL* (encoding CD62L, L-selectin), and *ITGAL* (encoding lymphocyte function-associated antigen-1 [LFA-1], receptor for intracellular adhesion molecule [ICAM]1) (Figure 2E). The expression for *ITGB1*, *CRTAM*, and *ITGAL* were higher and *SELL* expression was lower in *NRP1*$^+$ ILC3s compared with *NRP1*$^-$ ILC3s. β1-integrin, CD62L, and LFA-1 play important roles in lymphocyte migration, adhesion, and interaction with non-lymphoid cells (Carrasco et al., 2004; Evans et al., 2009). CRTAM is expressed by Purkinje neurons, epithelial cells, activated NKT cells, NK cells, and CD8 T cells. The interaction of CRTAM with its ligand Nelc-2 is reported to promote cell adhesion between both lymphoid and non-lymphoid cells (Garay et al., 2010). In addition, scRNA-seq revealed that NRP1$^+$ ILC3s expressed higher levels of the receptor for *ITGB1*, *ITGAL* (Figure 2E), *LTα*, and *LTβ* (Figure 2A), markers involved in the interaction between LTi cells with stromal cell. Enrichment of these pathways is indicative of the interaction between NRP1$^+$ ILC3s and non-hematopoietic stromal and/or endothelial cells. Together the scRNA-seq results indicate that *NRP1*/NRP1 may be involved in migration and/or retention of ILC3s in lymphoid tissue, and *NRP1*$^+$ ILC3s show a more mature and/or activated phenotype compared with *NRP1*$^-$ ILC3s.

NRP1-Positive ILC3s Resemble Primed Cells

Next, we analyzed the functional properties of NRP1$^+$ and NRP1$^-$ ILC3s. Assessing the cytokine production using intracellular flow cytometry of ex vivo tonsillar NRP1$^{+/-}$NKp44$^+$ ILC3s, stimulated

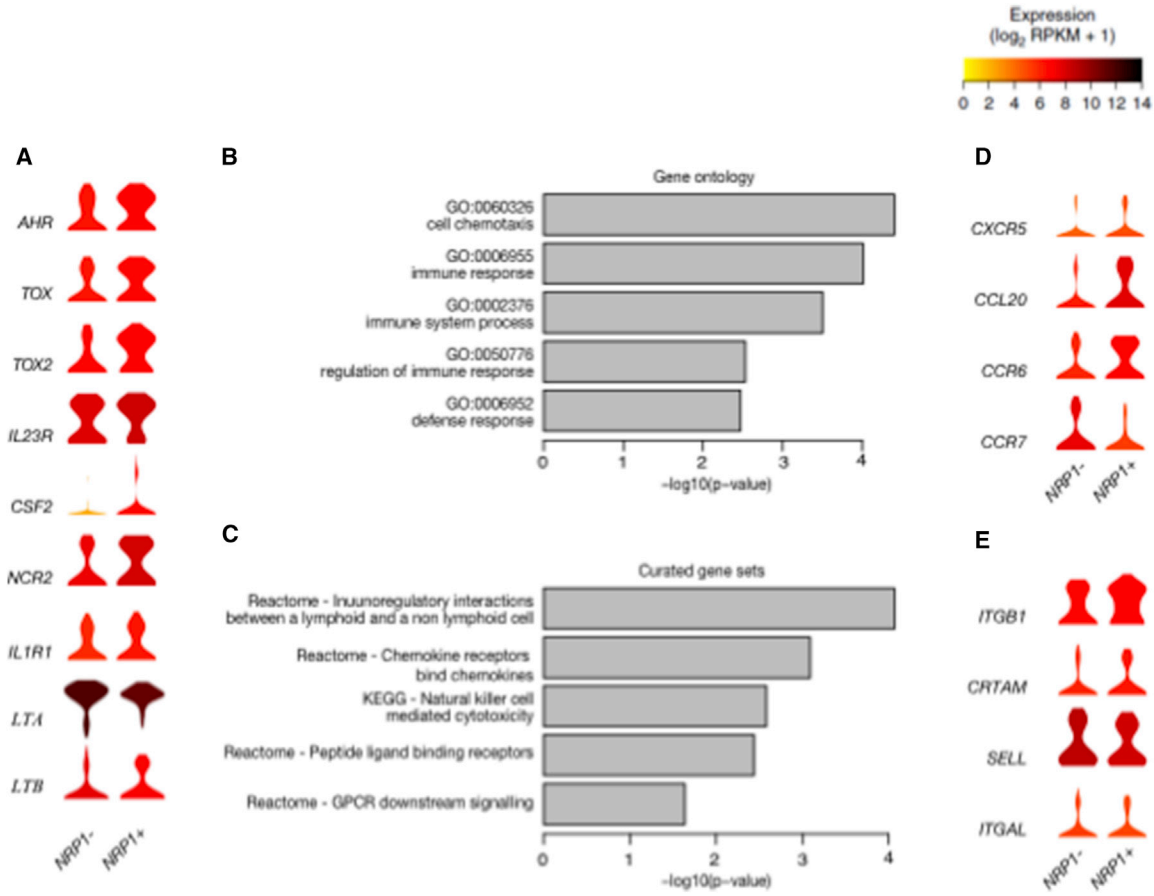

Figure 2. Violin Plots Showing the Gene Expression Distribution in *NRP1*$^+$ and *NRP1*$^-$ ILC3s

(A) Group 3 ILC3s signature genes. Violin plots show gene expression distribution in *NRP1*$^+$ and *NRP1*$^-$ ILC3s with color according to mean expression value.
(B and C) Bar plots with the top five enriched GO terms (B) and MSigDB curated gene sets (C) with bar height according to adjusted p value.
(D) Violin plots with genes in GO term "Cell chemotaxis, immune response."
(E) Violin plots with genes in Reactome pathway "Immunoregulatory interaction between a lymphoid and non-lymphoid cell."

with phorbol 12-myristate 13-acetate (PMA) plus ionomycin, revealed that NRP1$^+$ ILC3s produced significantly higher amounts of IL-22 compared with NRP1$^-$ ILC3s (Figure 3A), whereas neither subset produced IL-17A (data not shown). Following in vitro stimulation with IL-2 or with IL-2, IL-1β, and IL-23, NRP1$^+$ ILC3s produced 2- to 3-fold higher amounts of proinflammatory cytokines GM-CSF, TNF-α and the chemotactic and angiogenic factor IL-8, and lymphotoxin than NRP1$^-$ ILC3s as measured by ELISA in culture supernatants (Figure 3B). Both ILC3 populations produced similar amounts of lymphotoxin (LT)-α and the chemokines CXCL10, MIP-1α, and MIP-1β upon stimulation with IL-2, IL-1β, and IL-23 (data not shown). NRP1$^+$ ILC3s produced less IFN-γ compared with NRP1$^-$ ILC3s (Figure 3B). These data indicate that NRP1$^+$ ILC3s in general have the capacity to produce significantly more cytokines than NRP1$^-$ ILC3s. Similarly, stimulation of freshly isolated fetal lymph node NRP1$^+$ ILC3s with PMA plus ionomycin resulted in a significantly higher production of IL-22 and also higher IL-17A production by NRP1$^+$ ILC3s compared with NRP1$^-$ ILC3s (Figure 3C). One possible explanation for the higher production of cytokines by NRP1$^+$ ILC3s is that these cells have encountered an activation signal in vivo implying they may have been primed like is the case for memory T cells. Because CD45RA and CD45RO define naive and memory T cells, respectively, and naive T cells express CD62L, we analyzed the expression of these markers on the NRP1$^+$ and NRP1$^-$ ILC3 subsets. We observed that a minor population of tonsillar NKp44$^-$ NRP1$^-$ILC3s are CD45RA-positive, whereas tonsillar NRP1$^+$ ILC3s are negative for CD45RA (Figure 3D) and positive for CD45RO (Figure 3D).

We next asked which signal could be responsible for upregulation of NRP1 by ILC3s. Because IL-1β is a prominent stimulator of ILC and its receptor tended to be expressed to higher extent by *NRP1*$^+$ ILC3s as determined by scRNA-seq (Figure 2A), we tested whether IL-1β had an effect on expression of NRP1. We highly purified NRP1$^-$ ILC3s and observed that culturing these cells in IL-1β upregulated NRP1 (SD 27% ± 6%; Figure 3E). NRP1$^+$ ILC3s lost the expression of NRP1 in culture without additional stimuli and maintained NRP1 expression when stimulated with IL-1β (data not shown). Intriguingly, culture of peripheral blood ILC3s in IL-1β did not result in NRP1 upregulation

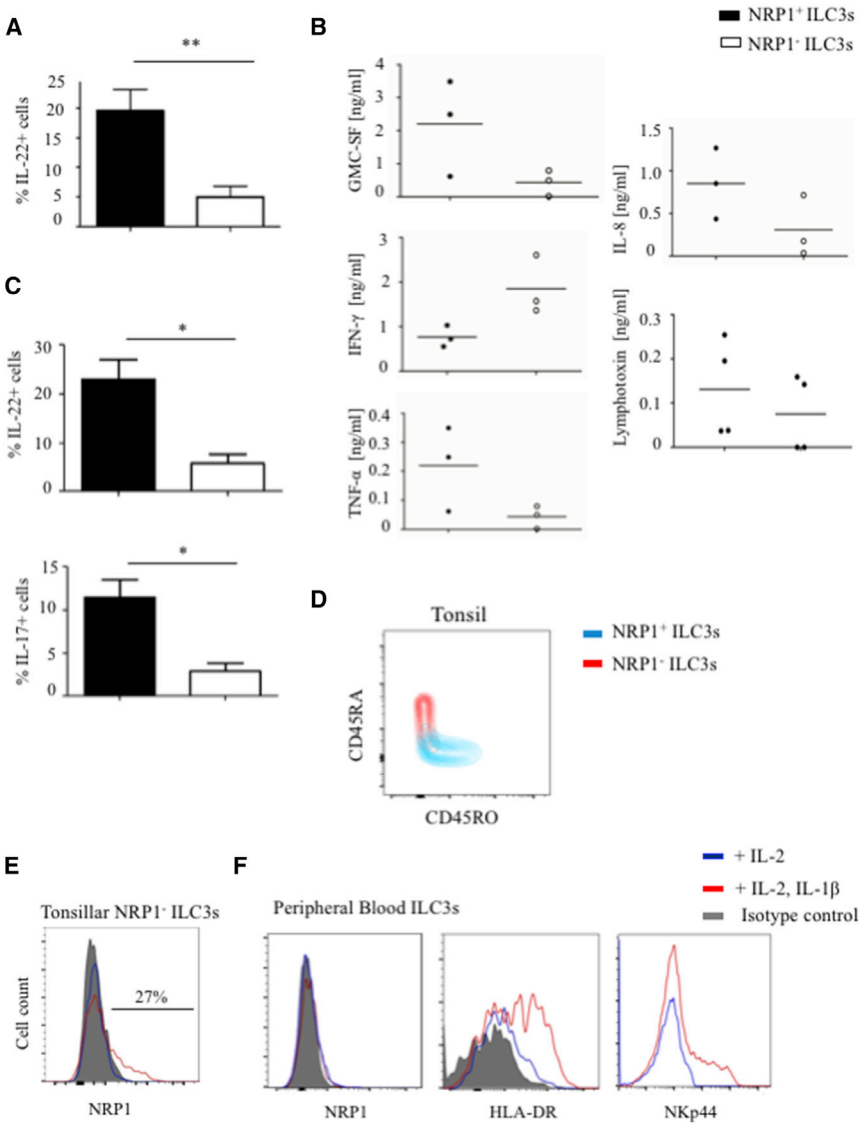

Figure 3. NRP1$^+$ ILC3s Express CD45RO and Produce Higher Amounts of Cytokines Than NRP1$^-$ ILC3s

(A) Freshly isolated ILC3s were in vitro stimulated with PMA plus ionomycin and analyzed for intracellular IL-22 (n = 4, *p < 0.05, Mann-Whitney two-tailed t test).

(B) Luminex bead-based assay was used to measure multiple cytokine secretion. Soluble GM-CSF (ng/mL) and TNF-α, IL-8, and IFN-γ from cultured and IL-2-, IL-1β-, and IL-23-stimulated ILC3s. Data are representative of three individual tonsil samples analyzed in different experiments; horizontal bars represent the median value for each group.

(C) Freshly isolated ILC3s from fetal mLN in vitro stimulated with PMA plus ionomycin and intracellular cytokine stain for IL-22 and IL-17A on NRP1$^+$ (black bar) and NRP1$^-$ (white bar) ILC3s, analyzed by flow cytometry (n = 4, *p < 0.05, Mann-Whitney two-tailed t test).

(D) CD45RA and CD45RO expression on NRP1$^+$ (red) and NRP1$^-$ (blue) ILC3s in tonsil.

(E and F) Histogram showing the expression of NRP1 on NRP1$^-$ ILC3s in tonsil (E) and NRP1, HLA-DR, and NKp44 on peripheral blood NRP1$^-$ ILC3s (F) after stimulation with IL-2 alone (blue lines) or with IL-2 and IL-1β (red lines). Filled histogram shows isotype control.

(Figure 3F). This was not due to the lack of responsiveness of peripheral blood ILC3s to IL-1β, because peripheral blood ILC3s upregulated class II MHC and NKp44 (Figure 3F) following incubation with IL-1β. Taken together, the high cytokine production capacity and the phenotype of NRP1$^+$ ILC3s suggest that these cells may represent previously primed cells.

A Role for NRP1 in the ILC3s Retention in Lymphoid Structures

We analyzed the expression of the major molecules that mediate the migration of lymphocytes to peripheral lymph nodes (Evans et al., 2009), such as CD62L, lymphocyte function-associated antigen-1 (LFA-1), CCR7, and CCR6, and found that ILC3s in the peripheral blood, which all are NRP1$^-$, expressed high levels of LFA-1 and CCR6, but lacked expression of CCR7 (Figure S2A). The majority of peripheral blood ILC3s expressed the adhesion molecule CD62L and a small population expressed CXCR5, suggesting that a subset of ILC3s can migrate to lymphoid tissue. Tonsillar ILC3s were CD62L$^-$, except for a minor population of NKp44$^-$ ILC3s (Figure 4A). Comparable with peripheral blood ILC3s, tonsillar ILC3s were LFA-1 high and lacked the expression of CCR7. Tonsillar NKp44$^+$ ILC3s expressed high levels of CCR6, whereas NKp44$^-$ ILC3s and ILC1 showed a heterogeneous expression of this chemokine receptor. Our data suggest that NRP1$^+$ ILC3s are exclusively present in lymphoid tissues under homeostatic conditions. To gain insight in the localization of NRP1$^+$ ILC3s within the lymphoid tissues, we performed double immunohistochemical (IHC) staining of tonsil tissue. In humans NRP1 is described as a selective marker for pDCs among the dendritic cells (DCs) and is also expressed by Treg cells in secondary lymphoid tissue and a subset of CD4$^+$ T follicular helper cells. Single IHC staining for CD3 (T cell specific), BDCA2 (pDC specific), and NRP1 was performed to validate the antibodies (Figures S2B–S2D). Quantifications using automated IHC and digital image analysis showed that NRP1$^+$ cells were present in different regions of the tonsil, including the follicular region (mantle zone and inner germinal center), paracortex, and medullar region. NRP1$^+$ cells were significantly increased in the paracortical region and medullar region (Figure S2E). However, in a co-IHC staining we excluded confounding T cells and pDCs with anti-CD3 and anti-BDCA2 antibodies (black chromogenic stain) followed by NRP1 staining (brown stain). The

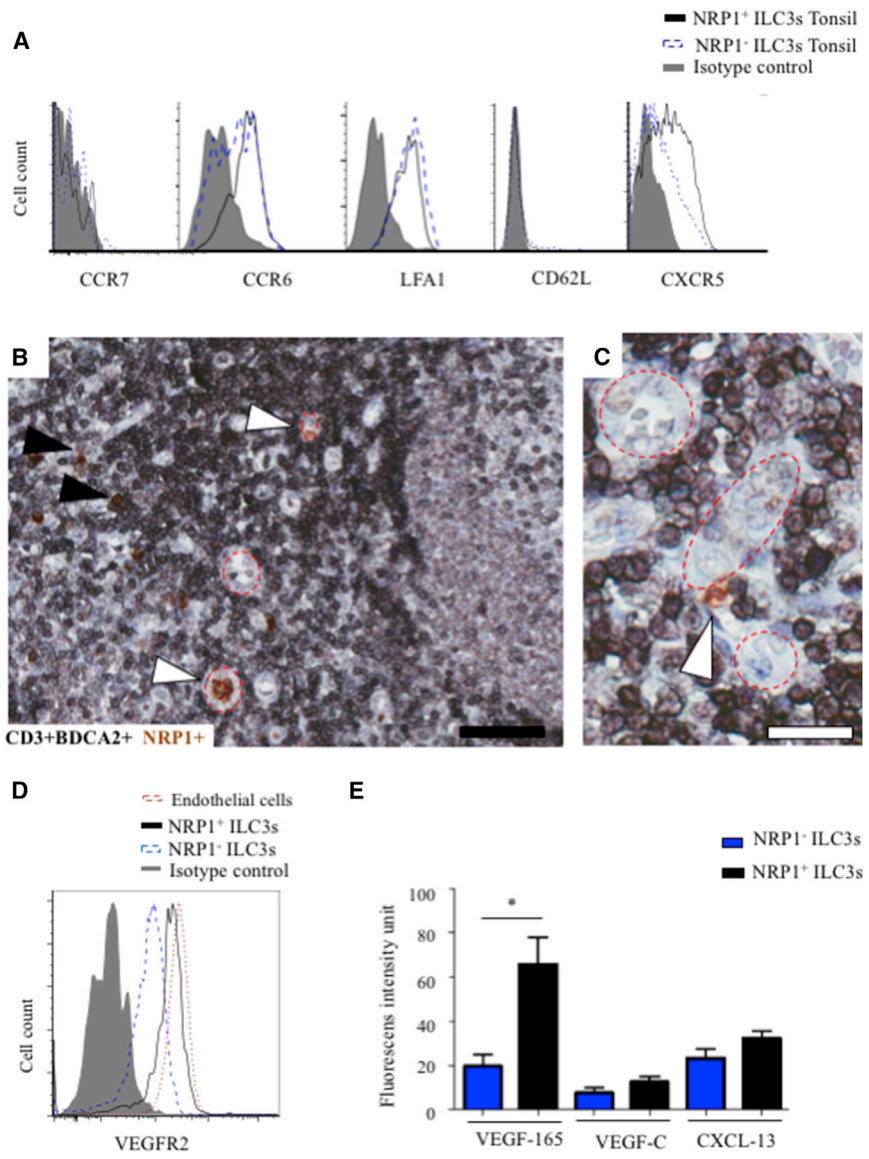

Figure 4. Tonsillar NRP1$^+$ ILC3s Are Detected in Proximity to HEVs and the NRP1 Ligand VEGF-A Serves as a Chemotactic Factor for NRP1$^+$ ILC3s

(A) Cell surface expression of CCR7, CCR6, LFA-1, CD62L, CXCR5, and NRP1 on freshly isolated ILC3s from tonsil, NRP1$^+$ ILC3s (black line), and NRP1$^-$ ILC3s (dark blue dashed line) assessed by flow cytometry. Filled histogram shows isotype control.

(B and C) Photomicrographs showing immunohistochemically (IHC) stained paraffin-embedded sections from two different donor tonsils. Tissue sections were double stained for NRP1$^+$ (brown stain) CD3$^-$BDCA2$^-$ (black stain). White arrowheads indicate NRP1$^+$BDCA2$^-$ cells, and black arrowheads indicate NRP1$^+$CD3$^+$BDCA2$^+$ pDCs. Dotted red lines show HEV-like structures. Black scale bar, 100 μm; white scale bar, 50 μm.

(D) VEGFR2 expression on NRP1$^+$ ILC3 (black line) and NRP1$^-$ ILC3s (dark blue dashed line) and positive control endothelial cells (red dashed line).

(E) Five-micrometer Transwell chemotaxis assay migratory/chemotaxis properties measured by fluorometric detection. Chemoattractants used were VEGFR2-NRP1 ligand VEGF-165 (VEGF-A), VEGFR2 ligand VEGF-C, and CXCR5 ligand CXCL13. NRP1$^+$ ILC3s chemotaxis toward VEGF-A (n = 5, SD 66 ± 12) and NRP1$^-$ ILC3s chemotaxis toward VEGF-A (n = 8, SD 20 ± 4.5), *p < 0.01. Baseline represents medium without chemoattractant.

staining revealed that the CD3$^-$BDCA2$^-$NRP1$^+$ cells were selectively located in proximity to structures that closely resemble high endothelial venules (HEVs) in paracortical regions and near HEVs in the proximity of the medullar region (Figures 4B and 4C).

VEGF-A Serves as a Chemotactic Factor for NRP1-Positive ILC3s

NRP1 and its co-receptor VEGFR2 have been implicated in the transendothelial migration of T cells and pDCs, and their localization at sites of inflammation (Edelbauer et al., 2010; Suzuki et al., 2014). We observed that NRP1$^-$ and NRP1$^+$ ILC3s expressed the co-receptor VEGFR2 at expression levels similar to that on endothelial cells (Figure 4D). The VEGF-A effect on endothelial cell migration has been shown in several studies (Lamalice et al., 2007). We therefore asked whether VEGF-A (isoform VEGF165) has an effect on the migration of ILC3s. We studied the migration of ILC by applying the chemoattractant to the lower Transwell chamber, mimicking typical chemo-attraction. Cells migrating into the lower chamber were analyzed after 12 hr of incubation, and spontaneous migration without chemoattractant was subtracted from the total (baseline, Figure 4E). Figure 4E shows that compared with NRP1$^-$ ILC3s, NRP1$^+$ ILC3s exhibited a significantly higher migration capacity, with a greater than 3-fold increase in migration toward VEGF-A. VEGF-C, which only binds VEGFR2 and not NRP1, had a similar moderate effect on both subsets (Figure 4E). These findings indicate that engagement of NRP1 in complex with VEGFR2 and not engagement of just VEGFR2 induces strong migration. The lack of effect of the VEGF-A on NRP1$^-$ ILC3s was not due to a general inability of these cells to migrate because NRP1$^-$ ILC3s did migrate toward VEGF-C and migrated toward the chemokine CXCL13 to a similar extent as NRP1$^+$ ILC3s (Figure 4E), possibly due to that a population within the NRP1$^-$ ILC3s also expresses CXCR5 (receptor for CXCL13; Figure 4A).

Cross-Talk of NRP1-Positive ILC3s with Mesenchymal Stromal Cells

Our observation that NRP1 is specifically expressed on ILC3s present in lymphoid tissues suggested it is a potential marker

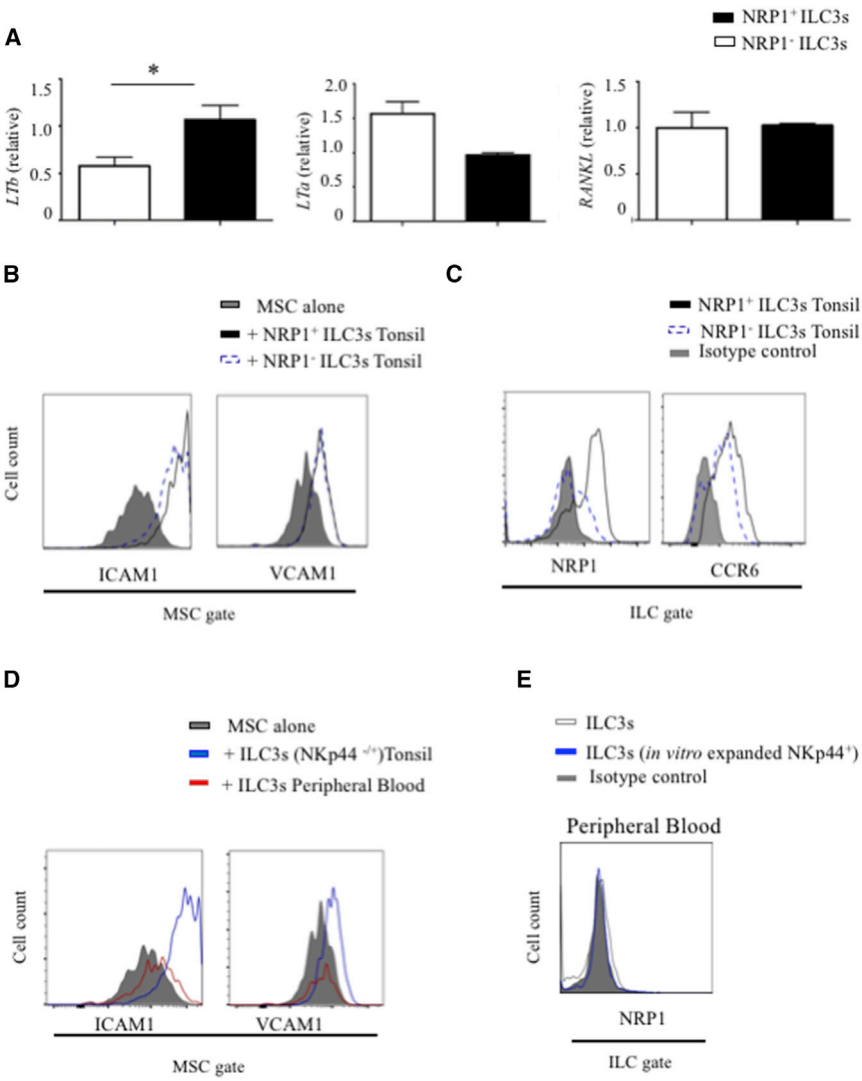

Figure 5. NRP1$^+$ ILC3s Exhibit In Vitro LTi Activity

(A) qRT-PCR of mRNAs for *LTA* (LT-α), *LTB* (LT-β), and *RANKL* in fetal mLN NRP1$^+$ and NRP1$^-$ ILC3s, normalized to mRNA encoding β-actin (*ACTB*). Data are represented as mean of four donors ± SD, *$p < 0.05$ (B-E). The functional lymphoid tissue inducing ability of lymphoid (fetal mLN, tonsil) and peripheral blood ILC3s was tested by induced expression of ICAM1 and VCAM1 on MSCs cultured alone or with ILC3s for 5 days.

(B) Tonsillar ILC3s co-cultured with MSCs, showing ICAM1 and VCAM1 expression on MSCs. MSCs co-cultured NRP1$^+$ ILC3s (black line), MSCs co-cultured NRP1$^-$ ILC3s (dark blue dashed line), and MSCs cultured alone (filled gray bar) are shown.

(C) NRP1 and CCR6 expression tonsillar ILC3s after co-cultured with MSC. Gray filled histogram shows isotype control and NRP1$^+$ (black line) and NRP1$^-$ (dark blue dashed line) ILC3s.

(D) ILC3s co-cultured with MSCs, showing ICAM1 and VCAM1 expression on MSCs. MSCs co-cultured freshly isolated peripheral blood ILC3s (red line), MSC co-cultured with tonsillar ILC3s (dark line), and MSCs cultured alone (filled gray bar) are shown.

(E) NRP1 expression on peripheral blood ILC3s after co-cultured with MSCs. Gray filled histogram shows isotype control, freshly isolated ILC3s (gray line), and in vitro expanded ILC3s (blue line).

for LTi cells. Recently, *NRP1* transcripts were reported to be expressed on adult murine CD4$^-$ ILC3s cells that have features of LTi cells (Robinette et al., 2015), but NRP1 expression has not yet been shown in mouse fetal LTi cells that actually induce lymphoid organogenesis (Robinette et al., 2015). Confocal microscopy analysis of fetal lymph nodes (embryonic day [E] 14.5 and E18.5 wild-type [WT]) in mouse embryo revealed NRP1 to be expressed in fetal CD4$^+$ LTi cells (Figure S3); NRP1 staining was not restricted to hematopoietic cells, because it was also detected on stromal cells and extracellular matrix.

It has been shown that lymphotoxin-α (LT-α) and lymphotoxin-β (LT-β) play a crucial and non-redundant role in the development of lymphoid organs (Drayton et al., 2006). Analysis of LTi hallmark gene expression by qRT-PCR showed that fetal NRP1$^+$ ILC3s expressed significantly higher levels of *LTβ* and comparable *RANKL* expression compared with NRP1$^-$ ILC3s (Figure 5A). Expression of *LTα* tended to be lower compared with NRP1$^-$ ILC3s, but this difference was not statistically significant. To test whether NRP1$^+$ ILC3s from fetal mLN and tonsil might function as LTi cells, we cultured these cells with mesenchymal stromal cells (MSCs) as we described before that fetal LTi cells induce VCAM1 and ICAM1 in a lymphotoxin beta receptor (LTβR)- and tumor necrosis factor receptor (TNFR)-dependent way (Cupedo et al., 2009). Co-culture of MSCs with both NRP1$^+$ and NRP1$^-$ ILC3s induced the expression of VCAM1 and ICAM1 on MSCs (Figure 5B), whereas no changes in CD73, CD90, and CD105 expression by the MSCs were observed upon co-culture with ILCs (data not shown). The observation that both NRP1$^+$ and NRP1$^-$ ILC3s could induce the expression of VCAM1 and ICAM1 on MSCs may not be consistent with the hypothesis that only NRP1$^+$ have LTi activity. However, we noted that the co-culture of highly purified fetal (data not shown) and tonsillar (Figure 5C) NRP1$^-$ ILC3s with MSCs resulted in upregulation of NRP1. NRP1$^-$ ILC3s did not express NRP1 in the absence of MSCs (data not shown). The expression of CCR6 was higher on NRP1$^+$ cells (Figure 5C), and RANKL and CD25 (data not shown) expression were similar on both ILC3 subsets after co-culture. The effects we observed on either MSCs or ILC3s were specific for tissue-derived ILC3s because peripheral blood ILC3s failed to upregulate expression of VCAM1 and ICAM1 on MSCs (Figure 5D), and NRP1 expression was not induced on peripheral blood ILC3s when co-cultured with MSCs (Figure 5E).

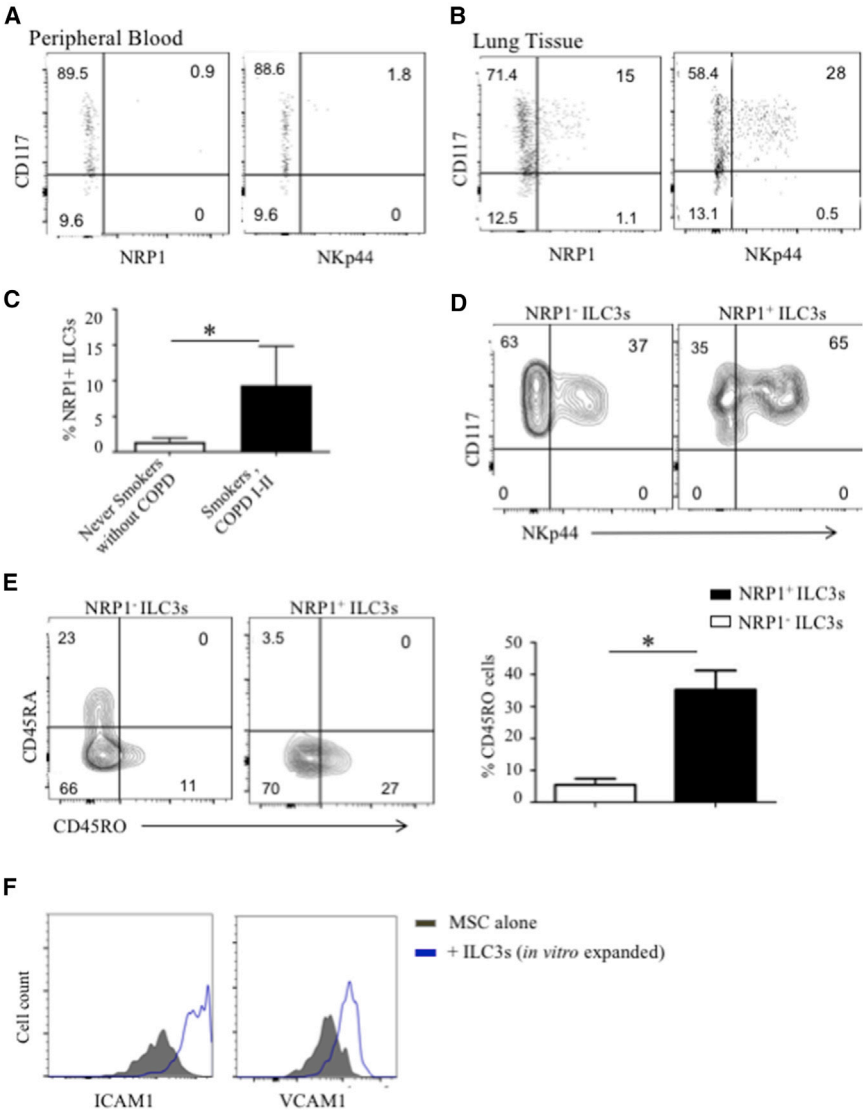

Figure 6. Primed NRP1$^+$ ILC3s Detected in the Lung Tissue of Smokers without COPD and COPD Patients

(A) NRP1 and NKp44 expression on ILC3s from peripheral blood of COPD patients.

(B) NRP1 and NKp44 expression on ILC3s from the lung tissue of COPD patients.

(C) Quantification of NRP1$^+$ ILC3s in never-smoking control patients (without COPD, n = 4, SD 1% ± 1% of total ILC3s) compared with smokers and COPD GOLD stage I–II patients (n = 4, SD 11% ± 5% of total ILC3, *p < 0.05).

(D) NKp44 and NRP1 on NRP1$^-$ and NRP1$^+$ lung tissue ILC3s.

(E) CD45RA and CD45RO expression on NRP1$^-$ and NRP1$^+$ COPD lung tissue ILC3s. Quantification of CD45RO$^+$ ILC3s (n = 4, *p = 0.03) is shown.

(F) In vitro expanded lung ILC3s co-cultured with MSCs, showing ICAM1 and VCAM1 expression on MSCs. MSCs co-cultured with ILC3s (blue line) or cultured alone (filled gray bar) are shown.

Both freshly isolated peripheral blood ILC3s and in-vitro-activated and expanded peripheral blood ILC3s failed to induce VCAM1 and ICAM1 on MSCs (Figure 5D), indicating that in contrast to lymphoid tissue ILC3s, peripheral blood ILC3s do not have LTi cell activities. The observation that NRP1 is upregulated in co-cultures with MSCs supports the notion that NRP1 is a marker for primed ILC3s with LTi activity. These results also indicate that lymphoid tissue and peripheral blood ILC3s have distinct functional properties.

Primed NRP1-Positive ILC3s in Lung Tissue of Smokers and Chronic Obstructive Pulmonary Disease Patients

The presence of NRP1$^+$ cells has previously been shown in lymphoid aggregates in the synovium of rheumatic arthritis patients (E et al., 2012), and ILC3s were recently detected in human non-small-cell lung cancer tissue, presumably linked to the formation of tumor-associated ectopic lymphoid neogenesis, also called tertiary lymphoid organ (Carrega et al., 2015). Ectopic lymphoid formations occur in peripheral and non-lymphoid tissues from patients with inflammatory and infectious disease, as well as autoimmune pathologies (Pitzalis et al., 2014; Carragher et al., 2008). In the lung, ectopic lymphoid aggregates (LAs) are observed in several lung diseases such as in the bronchioles of chronic obstructive pulmonary disease (COPD) patients (Hogg, 2004; Mori et al., 2013) and asthmatics (Elliot et al., 2004). Because LAs are rare in lungs of non-smokers (Tschernig and Pabst, 2000; Mori et al., 2013), LAs are considered to represent a form of inducible lymphoid structures associated with the severity of COPD (Brusselle et al., 2009; Mori et al., 2013). Several immune cell types including LTi cell, IL-17-secreting CD4$^+$ T cell, and T follicular helper cell have been implicated in the propagation of LA within inflamed tissue that is driven by communication among local stromal cells, tissue-specific resident mononuclear cells, and infiltrating immune cells (Carragher et al., 2008).

Therefore, we analyzed the composition of ILC3s subsets in peripheral blood and lung tissue of patients suffering from COPD. A subset of ILC3s in lung tissue from COPD patients (Global Initiative for Chronic Obstructive Lung Disease [GOLD] stages I–II) and smokers without COPD expressed NRP1 (Figure 6B), whereas peripheral blood ILC3s from the same patients lacked NRP1 (Figure 6A), and the number of NRP1$^+$ ILC3s was significantly reduced in never smokers without COPD (Figure 6C). The majority of NKp44$^+$ ILC3s expressed NRP1 (Figure 6D). Furthermore, the expression of CD45RO (Figure 6E) in COPD and smokers was significantly higher on NRP1$^+$ ILC3s when compared with NRP1$^-$ ILC3s. NRP1$^+$ ILC3s were CD45RA$^-$, whereas NRP1$^-$ ILC3s showed a heterogeneous

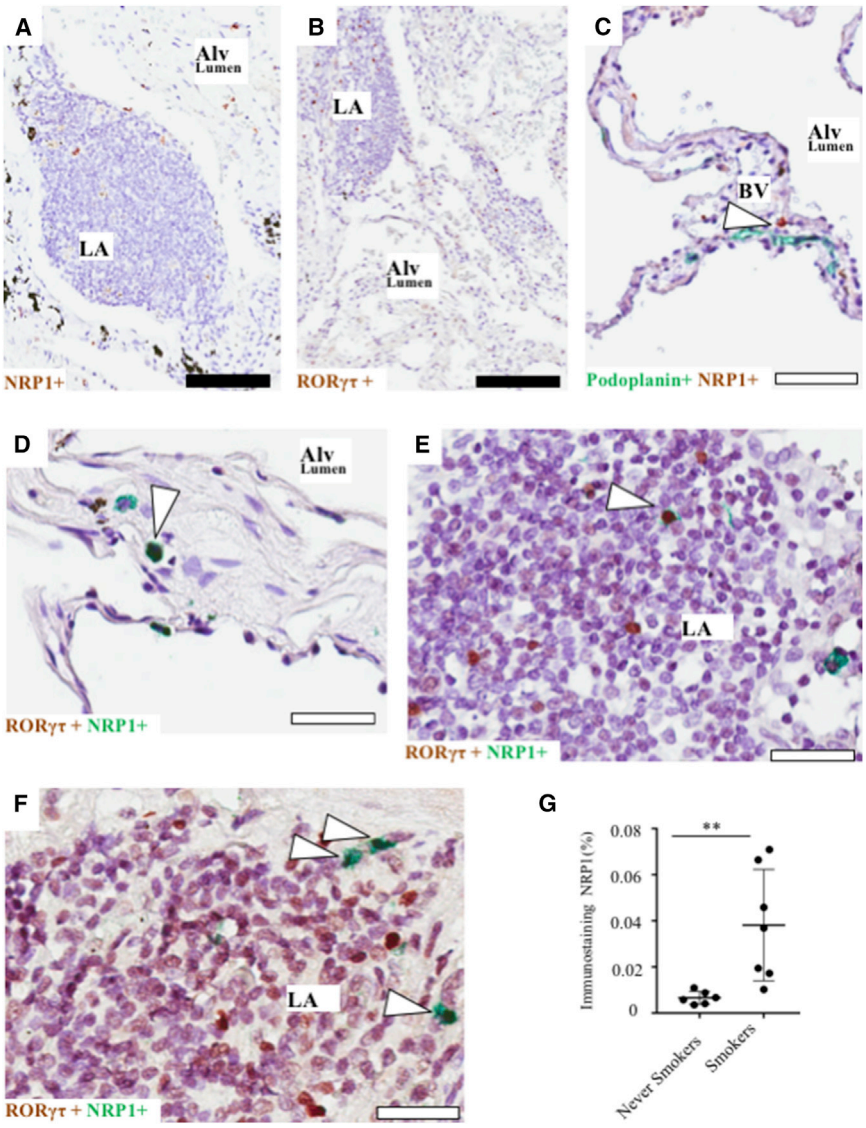

Figure 7. RORγt$^+$NRP1$^+$ Cells Located in Proximity to Pulmonary Blood Vessels and Ectopic Lymphoid Aggregates

(A) Bright-field micrograph of peripheral lung tissue showing NRP1 staining in alveolar (Alv) lumen and pulmonary lymphoid aggregate (LA). Black endogenous pigments are visible.

(B) Bright-field micrograph showing RORγt staining in alveolar lumen and LA.

(C) Double IHC staining for NRP1 (brown stain) and lymphatic vessel stained with podoplanin (blue-green stain) in alveolar lumen. White arrowheads indicate NRP1$^+$ cells in proximity to blood vessels (Bv).

(D–F) Double IHC staining for RORγt (brown stain) and NRP1 (blue-green stain) in (D) alveolar lumen and (E and F) in the surroundings of LAs. White arrowheads indicate RORγt$^+$NRP1$^+$ cells.

(G) Percentage of NRP1 immunostaining in the peripheral lung of never-smoking (n = 6) and smoking (n = 7) subjects with suspected bronchial tumor, quantified using image analysis program (**p < 0.01).

Black scale bars, 100 μm; white scale bars, 50 μm.

expression for this receptor. Co-culture of MSCs with in-vitro-expanded ILC3s (NRP1$^{-/+}$) isolated from lung tissues from COPD patients induced the expression of VCAM1 and ICAM1 on MSCs (Figure 6F), indicating that the ILC3s residing in the inflamed lung have LTi activity.

NRP1-Positive ILC3s Associated with Pulmonary Blood Vessels and Ectopic Lymphoid Aggregates

Next we explored the anatomic location of RORγt$^+$NRP1$^+$ ILC3s in peripheral lung resection samples obtained from COPD patients (with mild, moderate-to-severe, and very severe COPD) and patients without COPD undergoing surgery for suspected bronchial tumor. Asymptomatic patients had normal lung function and included never smokers and smokers. RORγt encodes a transcription factor that is expressed in interleukin-17 (IL-17)-producing cells, including CD4$^+$ T helper cells and group 3 ILCs. Single IHC staining with primary antibodies directed against NRP1 (Figure 7A; Figure S4A) and RORγt (Figure 7B; Figure S4B) showed similar expression patterns for NRP1$^+$ and RORγt$^+$ cells, where positive cells were present in the perivascular area (i.e., adjacent to pulmonary arteries and veins), the alveolar parenchyma, and ectopic lymphoid aggregates (LAs), often close to HEV-like vessels. Double IHC staining with anti-RORγt (brown stain) followed by anti-NRP1 staining (green stain) revealed that the vast majority of RORγt$^+$NRP1$^+$ cells were located in proximity to blood vessels and in the alveolar parenchyma (Figure 7D). Lymphatic endothelium was histologically distinguished from blood vessels by morphological criteria and detection of the pan-lymphatic vessel marker podoplanin (Figure 7C). Scarce numbers of RORγt$^+$NRP1$^+$ cells were also observed in or at the edge of LAs in smoking patients without COPD and COPD lung tissue (Figures 7E and 7F). In contrast with never-smoking patients with suspected bronchial tumor, LAs were readily detected in peripheral lungs of patients with COPD and smoking subjects without COPD. Next, we analyzed the expression levels of NRP1 immunostaining in never smokers and smokers without COPD, establishing whether elevated levels of these molecules are associated with smoke-induced pulmonary LA. Quantifications using automated IHC and digital image analysis, in line with an increase of NRP1$^+$ ILC3s in smokers and COPD patients compared with never smokers, showed a significant increase in overall NRP1$^+$ cells (Figure 7G) in smoking subjects compared with never-smoking subjects (**p < 0.01). Altogether, these results are suggestive of a role for

RORγt$^+$NRP1$^+$ ILC3s in the initial stages of LA formations and vascularization in the lungs.

DISCUSSION

ILC3s and LTi cells require RORγt (*RORC2*) expression and IL-7 for their development and function, but recent studies using promyelocytic leukaemia zinc finger (PLZF) fate-mapping mice indicate that their developmental trajectory is different (Constantinides et al., 2014; Ishizuka et al., 2016). Recently, Nrp1 was shown to be selectively expressed on mouse intestinal CCR6$^+$ ILC3s considered to be LTi cells (Robinette et al., 2015). Here we confirm that NRP1 is expressed on the majority of CD4$^+$ LTi cells present in the developing lymph nodes of mice. Together these data indicate that NRP1 is a marker for mouse LTi cells.

In this study, we found that NRP1 is also associated with LTi cells in humans. We demonstrate that NRP1 is expressed only on ILC3s present in lymphoid tissues. NRP1$^+$ ILC3s upregulated VCAM1 and ICAM1 on MSCs, which is considered to be a surrogate assay for LTi activity in humans. Lymphoid tissue-residing NRP1$^-$ ILC3s also had LTi activity, but during co-culture with MSCs these cells acquired NRP1. In contrast, peripheral blood ILC3s, which lack NRP1, were unable to induce VCAM1 and ICAM1 on MSCs. Thus, only ILC3s that can acquire NRP1 or already express NRP1 have LTi activity. ILC3s that are negative for NRP1 and unable to upregulate NRP1 either by IL-1β or by co-culture with MSCs are distinct from LTi cells. An obvious candidate for the induction of NRP1 in co-culture with MSCs is IL-1β. However, antibodies against IL-1β did not inhibit induction of NRP1 in co-cultures with MSCs, and IL-1β is not detected in these co-cultures. Thus, the mechanism of induction of NRP1 by MSC remains to be elucidated.

Although both NRP1$^-$ and NRP1$^+$ tonsillar ILC3s have LTi activities, phenotypic comparison of tonsillar and fetal mLN NRP1$^+$ and NRP1$^-$ ILC3s combined with scRNA-seq revealed differences between these populations. NRP1$^+$ ILC3s produced significantly more ILC3 signature cytokines, such as IL-22 and GM-CSF, following in vitro stimulation. Moreover, NRP1$^+$ ILC3s express CD45RO and lack expression of CD45RA, CD62L, and CCR7. Together these data indicate that like CD45RO$^+$ memory T cells, NRP1$^+$ ILC3s are primed cells that had previously encountered an activation signal. IL-1β may be a signal that is responsible for priming of tonsillar LTi cells because this cytokine strongly upregulated NRP1 on NRP1$^-$ ILC3s. IL-1β was unable to upregulate NRP1 on peripheral blood ILC3s, which was not due to an inability of IL-1β to induce a signal in these cells because IL-1β induced class II MHC and NKp44 expression on peripheral blood ILC3s consistent with the notion that lymphoid tissue LTi cells are different from ILC3s in the circulation and non-lymphoid tissues. The reason why NRP1 cannot be induced on peripheral blood ILC3s by IL-1β is unclear. It is possible that as a consequence of different developmental pathways of these cells, the NRP1 locus is not in an open conformation in peripheral blood ILC3s or that signaling molecules that couple the IL-1β receptor to the NRP1 locus are absent in these cells.

That NRP1$^+$ ILC3s are primed, functional LTi cells is supported by analysis of single-cell transcriptomes of the *NRP1*-positive and -negative ILC3 populations. This analysis revealed in NRP1$^+$ cells enrichment of genes involved in "chemotaxis" and "lymphoid-non-lymphoid cell interaction" pathways, indicative of their interaction with non-hematopoietic stromal and endothelial cells. Moreover, IHC and flow cytometry analysis demonstrate that the NRP1$^+$ ILC3s are localized in the proximity of HEVs and express high levels of lymphocyte migration markers associated with chemotaxis to secondary lymphoid tissues. It is possible that migration of LTi cells is driven by VEGF-A because of our demonstration of VEGF-A being a chemotactic factor for NRP1$^+$ ILC3s in vitro. This potent proinflammatory factor is expressed at high levels in many chronic inflammatory diseases (Folkman, 1995). Maybe this pathway functions to recruit NRP1$^+$ ILC3s to sites of strong inflammation, for example, to mediate repair of tissues damaged by inflammation or to induce formation of lymphoid aggregates with the goal to resolve the inflammation.

Long-term exposure to cigarette smoke is the most important risk factor for developing COPD (Rabe et al., 2007). Cigarette smoke disrupts the physical epithelial barrier and activates epithelial cells to secrete several inflammatory cytokines and chemokines including IL-1β, IL-6, IL-8, and TGF-β (Kuschner et al., 1996; Yang et al., 2012). The inflammatory process in COPD involves both innate and immune cells, including infiltration of neutrophils, macrophages, cytotoxic CD8$^+$ T cells, as well as accumulation of B cells in severe COPD (Thorley and Tetley, 2007; Chung and Adcock, 2008). ILCs may also be involved in the pathology of COPD because ILC2s decrease and ILC1s are elevated in the inflamed COPD lungs (Bal et al., 2016; Silver et al., 2016). The elevation of ILC1s is correlated with the severity of the disease and is caused mainly by IL-12- and IL-18-induced transdifferentiation of ILC2s to ILC1 (Bal et al., 2016; Silver et al., 2016). ILC1 strongly contributes to the inflammation by enhanced production of IFN-γ. Also, ILC3 numbers were reported to be increased in COPD patients compared with control individuals (De Grove et al., 2016). NRP1$^+$ LTi cells might be responsible for the increased number of pulmonary ectopic LAs found in COPD patients (Hogg, 2004). Indeed, increased numbers of NRP1$^+$ CD45RO$^+$ ILC3s, which induced VCAM1 and ICAM1 on MSCs in vitro, were present in smokers and COPD patients compared with never smokers (without COPD). RORγt$^+$NRP1$^+$ ILC3s were located in the proximity to pulmonary blood vessels. Scattered RORγt$^+$NRP1$^+$ ILC3s cells were also observed adjacent to LAs. Altogether these results suggest that NRP1$^+$ ILC3s may be involved in initial stages of smoke-induced pulmonary LA formation and vascularization.

Previous studies have identified several factors that may contribute to the formation of pulmonary LAs such as pDCs (Van Pottelberge et al., 2010), CXCL13, and LT-β (Bracke et al., 2013; Litsiou et al., 2014). Interestingly, NRP1$^+$ ILC3s expressed high levels of migratory chemokine receptors, including CXCR5 (the receptor for CXCL13) and CCR6, which may be involved in the attraction of ILC3s to LA in the lung. Both IL-17A and IL-22, which are produced by ILC3s, play a crucial role in the formation of cigarette-smoke-induced lymphoid neogenesis (Roos et al., 2015) and are linked to ectopic lymphoid aggregate formation (Barone et al., 2015), respectively.

NRP1$^+$ ILC3s may also contribute to angiogenesis through IL-8 production (Vacca et al., 2015), VEGF-A responsiveness,

and activation of blood vessel endothelium. VEGF-A has been associated with lung inflammation, and the VEGFA-VEGFR2 receptor signaling is disturbed in the lungs of patients with COPD (Marwick et al., 2006), but how this affects recruitment of NRP1$^+$ ILC3s to inflamed lungs of COPD patients remains to be investigated. Overexpression of VEGF-A in the mouse results in type 2 immune-cell-mediated reactions including eosinophilic inflammation, mucous metaplasia, and airway hyperactivity (Lee et al., 2011), but it is yet unknown whether this involves NRP1$^+$ ILC3s. Identification of NRP1 as a marker of functional human LTi cells will now enable more detailed studies addressing whether these cells are involved in inflammation and how they contribute to vascularization and the initiation of ectopic lymphoid aggregates in chronic inflammatory and autoimmune diseases and in cancer.

EXPERIMENTAL PROCEDURES

Tissues, Isolation of Cells, and Study Cohort

Human fetal tissues were obtained from elective abortions contingent on the receipt of informed consent. Lymph nodes were dissected from the mesentery with dissecting microscopes. Tonsils were obtained from routine tonsillectomies, and use was contingent on the receipt of informed consent. Peripheral blood (healthy volunteers) was obtained from the blood bank at Sanquin. Tonsil tissue was cut in small pieces and mechanically disrupted using the Stomacher 80 Biomaster. Cell suspensions were filtered through a 70-μm cell strainer, and mononuclear cells were isolated with Ficoll-Paque Plus medium (GE Healthcare). Peripheral blood mononuclear cells from buffy coats and COPD patients were isolated by Ficoll-Hypaque density gradient separation and immunomagnetic bead selection (Miltenyi Biotech). Lung tissue cells were isolated by incubation of cut tissues with DNase I (50 U/mL; Sigma-Aldrich) and collagenase type 1 (300 U/mL; Worthington). Cell suspensions were passed through a 70-μm nylon cell strainer, and mononuclear cells were isolated with Lymphoprep (Axis-Shield). Lung tissues and peripheral blood for flow cytometric analysis were obtained with informed consent from adult patients with COPD (Global Initiative for Chronic Obstructive Lung Disease [GOLD] stages I–II) undergoing lung tumor surgery; tissues were obtained at an appropriate distance from the tumor. Study protocols were approved by the Academic Medical Center Medical Ethical Committee (Amsterdam). Peripheral lung tissues resections for histological study were collected at Skåne University hospital (Lund), and clinical characteristics of the study cohort are further described by Mori et al. (2013). In brief, according to the GOLD criteria (Rabe et al., 2007), n = 13 patients at GOLD stages I–II and n = 11 patients at GOLD stages III–IV were included in this study cohort. Lung resections from subjects without COPD and with normal lung function included never smokers (n = 6) or smokers (current and ex-smokers; n = 7) without COPD. The study was approved by the Swedish Research Ethics Committee in Lund, and all patients signed informed consent.

Flow Cytometry Analysis

The following antibodies to human proteins were used: from BioLegend, fluorescein isothiocyanate (FITC)-conjugated anti-CD3 (OKT3), anti-CD14 (HCD14), anti-CD16 (3G8), anti-CD19 (HIB19), anti-CD34 (581), anti-CD94 (DX22), anti-CD123 (6H6), anti-FcER1α (Fc epsilon receptor I alpha) (AER-37); phycoerythrin (PE)-conjugated anti-ICOS (CD278, C398.4A), anti-NKp44 (P44-8), anti-VEGFR2 (7D4-6); brilliant violet (BV) 421-conjugated anti-CD161 (HP-3G10), BV421 anti-CD45RO (UCHL1); allophycocyanin (APC)-conjugated anti-CCR6 (29-2L17), anti-CCR7 (4B12), anti-CXCR5 (J252D4), anti-LFA-1 (M17/4), anti-NRP1 (12C2), and APC-cy7 anti-CD45RA (HI100); from BD Biosciences, PE-CF594-conjugated anti-CD3 (UCHT1) and anti-CD62L (DREG-56); from Becton Dickinson: FITC-conjugated anti-CD34 (581), anti-TCRαβ (IP26), and TCRγδ (B1); from Beckman Coulter, phycoerythrin-Cy7-conjugated anti-CD127 (R34.34) and PE Cy5.5-conjugated anti-CD117 (104D2D1); and from Miltenyi, PE-conjugated anti-NRP1 (AD5-17F6). For phenotypic analyses by flow cytometry, data were collected with an LSRFortessa instrument (BD Biosciences) and analyzed with FlowJo software (Tree Star).

Quantitative Real-Time PCR

Total RNA was isolated with a NucleoSpin RNA XS kit (Macherey-Nagel) according to the manufacturer's protocol. cDNA was synthesized with the High-Capacity cDNA Archive kit (Applied Biosystems). PCR was done on Bio-Rad iCycles (Bio-Rad) with SYBR Green I master mix (Roche). Bio-Rad CFX manager 3.1 software was used to quantify expression. All samples were normalized to the expression of Actin B (ACTB), and results are presented in a.u.

RNA Sequencing Analysis

Single-cell RNA-seq expression was obtained as reads per kilobase gene model and million mappable reads (RPKMs) from the Björklund, Forkel et al. (Björklund et al., 2016) expression matrix at GEO: GSE70580. Cells with expression of *NRP1* with RPKM > 1 were defined as *NRP1*-positive cells. To define the *NRP1*-negative set of cells, we had to remove the ones that group with *NRP1*$^+$ cells, but do not express the *NRP1* transcript, possibly because of technical drop-outs or stochastic gene expression. Thus, all cells that had closest pairwise Pearson correlation to a cell expressing *NRP1* were defined as putative *NRP1*$^+$ cell and excluded from the analysis. To define the set of genes that have similar expression pattern to NRP1, we used the genes with highest contribution to the negative principal component 2 (PC2) in a PCA with all the ILC3 transcriptomes. The set of top 100 genes along negative PC2 were subjected to a Fisher's test for enrichment in gene sets from Gene Ontology (GO) annotations (Reference Genome Group of the Gene Ontology Consortium, 2009) and curated gene sets from MSigDB (Subramanian et al., 2005). All analysis and plotting of scRNA-seq data were performed with the R software.

Cell Cultures and Analysis of Cytokine Production

Sorted ILCs were seeded at densities of 5,000–10,000 cells in round-bottom 69-well plates cultured in Yssel's medium (in-house-prepared) supplemented with 1% human AB serum. Freshly isolated ILCs were stimulated for 5 days using recombinant cytokines IL-2 (10 U/mL; Novartis) or IL-2, IL-1β (50 ng/mL; R&D Systems), and IL-23 (50 ng/mL; R&D Systems). Multiple cytokine production was measured using MILLIPLEX MAP human cytokine and chemokine magnet from Millipore. Highly purified ILC3s from fetal mLN or tonsil were co-cultured with MSCs from adult bone marrow as described before (Maijenburg et al., 2012), and cell surface markers were analyzed after 5 days of co-culture. Freshly isolated ILC3s were stimulated for 6 hr with PMA (10 ng/mL; Sigma) and ionomycin (500 nM; Merck) in the presence of GolgiPlug (BD Biosciences) for the final 2 hr of culture. A Cytofix/Cytoperm kit (BD Biosciences) was used for cell fixation and permeabilization, followed by intracellular staining with conjugated anti-IL-22 and anti-IL-17A. Data were acquired on an LSRFortessa instrument and analyzed with FlowJo software.

Chemotaxis Assay

ILC migratory effect was assessed ex vivo using CytoSelect 96-well Cell Migration Assay, in 5 μm pore size Transwell plates (Cell Biolabs). Uncoated Transwell inserts were placed in Yssel's medium (1% human serum) containing recombinant protein VEGF-165 (25 ng/mL; BioLegend) or VEGF-C (50 ng/mL) or CXCL13 (200 ng/mL; BioLegend). A solution of ILC (20,000 in 0.1 mL of serum-free Yssel's medium) was added to the upper well of the Transwell, followed by 12 hr incubation at 37°C. Following CytoSelect Cell Migration manufacturer protocol, migratory cells were lysed and stained with fluorescence dye, followed by quantification of chemotaxis activity using fluorescence plate reader (BMG Polarstar; MTX Lab Systems).

Immunohistochemical Assessment

Sections were immunostained with EnVision Peroxidase/DAB (3,3′-Diaminobenzidine) Detection System kit (Rabbit/Mouse K5007; Dako). In double immunostaining, DAB staining was followed by the detection of the second antibody with Deep Space Black Chromogen kit (BRR807AH; Biocare Medical) or Vina Green Chromogen kit (BRR807AS; Biocare Medical). The sections

were incubated with Double Stain Blocking reagent (Dako A/S) to prevent additional binding of secondary antibody to primary antibody. Sections were counterstained with Mayer's hematoxylin (purple stain) after completion of IHC staining and mounted with Pertex. The following antibodies were used: CD3 (clone F7.2.38; Dako), BDCA2 (clone 104C12.08; Dendritics), RORγt (clone 6F3.1; Merck), podoplanin (clone D2-40; Biocare Medical), and NRP1 (LS-C177530; LifeSpan). NRP1$^+$ ILC3s in tonsil sections were identified as NRP1-positive cells (DAB HRP chromogen) after physical chromogen exclusion of CD3 and BDCA2-positive cells (Deep Space Black Chromogen). In the lung resection from COPD patients and control subjects, RORγt$^+$NRP1$^+$ ILC3s were identified as nuclear RORγt$^+$ (DAB HRP chromogen kit) and surface NRP1$^+$ (Vina Green chromogen kit) cells. Staining procedures were performed in an automated slide stainer (Autostainer Plus; DakoCytomation). Morphometric measurements of bright-field sections were performed using automated computerized image analysis program Aperio ImageScope V.10.0 software (Aperio Technologies). The percentage of NRP1 immunostainings was quantified as percentage of total number of positive pixels relative to total lung tissue (automatically excluding non-tissue areas) using the Aperio Positive Pixel Count Algorithm v.9 (Aperio Technologies).

Statistical Analysis

Statistical significance between two groups was determined by non-parametric, Mann-Whitney *U* test, using GraphPad Prism 6 (GraphPad Software).

SUPPLEMENTAL INFORMATION

Supplemental Information includes four figures and can be found with this article online at http://dx.doi.org/10.1016/j.celrep.2017.01.063.

AUTHOR CONTRIBUTIONS

M.M.S. designed the study, did experiments, analyzed the data, and wrote the manuscript. H.S. designed the study, analyzed data, and wrote the manuscript. Å.K.B. did experiments and analyzed the data. J.M. and B.B. analyzed data and wrote the manuscript. X.R.R., S.M.B., M.B., R.E.M., J.J.K., and A.S.C. did experiments. J.S.E. provided clinical material, and J.S.E. and M.M. provided concepts and resources for pulmonary IHC staining.

ACKNOWLEDGMENTS

We thank K. Weijer and J. Eder for help with processing fetal material, B. Hooibrink for help with flow cytometry, R. Lutter and R.E. Jonkers for providing COPD lung tissue, B. Dierdorp and T. Dekker for processing lung tissue, and J. Fergusson for critical reading of the manuscript. H.S. is supported by an advanced European Research Council grant (341038). A.S.C. is supported by the Landsteiner Foundation for Blood Transfusion Research (LSBR Fellowship 1101), and J.J.K. was supported by an A.L.W. program grant (820.02.004).

Received: August 29, 2016
Revised: November 9, 2016
Accepted: January 24, 2017
Published: February 14, 2017

REFERENCES

Artis, D., and Spits, H. (2015). The biology of innate lymphoid cells. Nature *517*, 293–301.

Bal, S.M., Bernink, J.H., Nagasawa, M., Groot, J., Shikhagaie, M.M., Golebski, K., van Drunen, C.M., Lutter, R., Jonkers, R.E., Hombrink, P., et al. (2016). IL-1β, IL-4 and IL-12 control the fate of group 2 innate lymphoid cells in human airway inflammation in the lungs. Nat Immunol. *17*, 636–645.

Barone, F., Nayar, S., Campos, J., Cloake, T., Withers, D.R., Toellner, K.M., Zhang, Y., Fouser, L., Fisher, B., Bowman, S., et al. (2015). IL-22 regulates lymphoid chemokine production and assembly of tertiary lymphoid organs. Proc. Natl. Acad. Sci. USA *112*, 11024–11029.

Bernink, J.H., Krabbendam, L., Germar, K., de Jong, E., Gronke, K., Kofoed-Nielsen, M., Munneke, J.M., Hazenberg, M.D., Villaudy, J., Buskens, C.J., et al. (2015). Interleukin-12 and -23 control plasticity of CD127+ group 1 and group 3 innate lymphoid cells in the intestinal lamina propria. Immunity *43*, 146–160.

Björklund, Å.K., Forkel, M., Picelli, S., Konya, V., Theorell, J., Friberg, D., Sandberg, R., and Mjösberg, J. (2016). The heterogeneity of human CD127 innate lymphoid cells revealed by single-cell RNA sequencing. Nat. Immunol. *17*, 451–460.

Bracke, K.R., Verhamme, F.M., Seys, L.J., Bantsimba-Malanda, C., Cunoosamy, D.M., Herbst, R., Hammad, H., Lambrecht, B.N., Joos, G.F., and Brusselle, G.G. (2013). Role of CXCL13 in cigarette smoke-induced lymphoid follicle formation and chronic obstructive pulmonary disease. Am. J. Respir. Crit. Care Med. *188*, 343–355.

Brusselle, G.G., Demoor, T., Bracke, K.R., Brandsma, C.A., and Timens, W. (2009). Lymphoid follicles in (very) severe COPD: beneficial or harmful? Eur. Respir. J. *34*, 219–230.

Carragher, D.M., Rangel-Moreno, J., and Randall, T.D. (2008). Ectopic lymphoid tissues and local immunity. Semin. Immunol. *20*, 26–42.

Carrasco, Y.R., Fleire, S.J., Cameron, T., Dustin, M.L., and Batista, F.D. (2004). LFA-1/ICAM-1 interaction lowers the threshold of B cell activation by facilitating B cell adhesion and synapse formation. Immunity *20*, 589–599.

Carrega, P., Loiacono, F., Di Carlo, E., Scaramuccia, A., Mora, M., Conte, R., Benelli, R., Spaggiari, G.M., Cantoni, C., Campana, S., et al. (2015). NCR(+) ILC3 concentrate in human lung cancer and associate with intratumoral lymphoid structures. Nat. Commun. *6*, 8280.

Chung, K.F., and Adcock, I.M. (2008). Multifaceted mechanisms in COPD: inflammation, immunity, and tissue repair and destruction. Eur. Respir. J. *31*, 1334–1356.

Constantinides, M.G., McDonald, B.D., Verhoef, P.A., and Bendelac, A. (2014). A committed precursor to innate lymphoid cells. Nature *508*, 397–401.

Cupedo, T., Crellin, N.K., Papazian, N., Rombouts, E.J., Weijer, K., Grogan, J.L., Fibbe, W.E., Cornelissen, J.J., and Spits, H. (2009). Human fetal lymphoid tissue-inducer cells are interleukin 17-producing precursors to RORC+ CD127+ natural killer-like cells. Nat. Immunol. *10*, 66–74.

De Grove, K.C., Provoost, S., Verhamme, F.M., Bracke, K.R., Joos, G.F., Maes, T., and Brusselle, G.G. (2016). Characterization and quantification of innate lymphoid cell subsets in human lung. PLoS ONE *11*, e0145961.

Drayton, D.L., Liao, S., Mounzer, R.H., and Ruddle, N.H. (2006). Lymphoid organ development: from ontogeny to neogenesis. Nat. Immunol. *7*, 344–353.

E, X.Q., Meng, H.X., Cao, Y., Zhang, S.Q., Bi, Z.G., and Yamakawa, M. (2012). Distribution of regulatory T cells and interaction with dendritic cells in the synovium of rheumatoid arthritis. Scand. J. Rheumatol. *41*, 413–420.

Edelbauer, M., Datta, D., Vos, I.H., Basu, A., Stack, M.P., Reinders, M.E., Sho, M., Calzadilla, K., Ganz, P., and Briscoe, D.M. (2010). Effect of vascular endothelial growth factor and its receptor KDR on the transendothelial migration and local trafficking of human T cells in vitro and in vivo. Blood *116*, 1980–1989.

Elliot, J.G., Jensen, C.M., Mutavdzic, S., Lamb, J.P., Carroll, N.G., and James, A.L. (2004). Aggregations of lymphoid cells in the airways of nonsmokers, smokers, and subjects with asthma. Am. J. Respir. Crit. Care Med. *169*, 712–718.

Evans, R., Patzak, I., Svensson, L., De Filippo, K., Jones, K., McDowall, A., and Hogg, N. (2009). Integrins in immunity. J. Cell Sci. *122*, 215–225.

Folkman, J. (1995). Angiogenesis in cancer, vascular, rheumatoid and other disease. Nat. Med. *1*, 27–31.

Garay, E., Patiño-López, G., Islas, S., Alarcón, L., Canche-Pool, E., Valle-Rios, R., Medina-Contreras, O., Granados, G., Chávez-Munguía, B., Juaristi, E., et al. (2010). CRTAM: a molecule involved in epithelial cell adhesion. J. Cell. Biochem. *111*, 111–122.

Hogg, J. (2004). Peripheral lung remodelling in asthma and chronic obstructive pulmonary disease. Eur. Respir. J. *24*, 893–894.

Ishizuka, I.E., Chea, S., Gudjonson, H., Constantinides, M.G., Dinner, A.R., Bendelac, A., and Golub, R. (2016). Single-cell analysis defines the divergence between the innate lymphoid cell lineage and lymphoid tissue-inducer cell lineage. Nat. Immunol. *17*, 269–276.

Killig, M., Glatzer, T., and Romagnani, C. (2014). Recognition strategies of group 3 innate lymphoid cells. Front. Immunol. *5*, 142.

Kuschner, W.G., D'Alessandro, A., Wong, H., and Blanc, P.D. (1996). Dose-dependent cigarette smoking-related inflammatory responses in healthy adults. Eur. Respir. J. *9*, 1989–1994.

Lamalice, L., Le Boeuf, F., and Huot, J. (2007). Endothelial cell migration during angiogenesis. Circ. Res. *100*, 782–794.

Lee, C.G., Ma, B., Takyar, S., Ahangari, F., Delacruz, C., He, C.H., and Elias, J.A. (2011). Studies of vascular endothelial growth factor in asthma and chronic obstructive pulmonary disease. Proc. Am. Thorac. Soc. *8*, 512–515.

Litsiou, E., Semitekolou, M., Galani, I., Morianos, I., Tsoutsa, A., Kara, P., Rontogianni, D., Bellenis, I., Konstantinou, M., Potaris, K., et al. (2014). Reply: CXCL13 in tertiary lymphoid tissues: sites of production are different from sites of functional localization. Am. J. Respir. Crit. Care Med. *189*, 370–371.

Maijenburg, M.W., Kleijer, M., Vermeul, K., Mul, E.P., van Alphen, F.P., van der Schoot, C.E., and Voermans, C. (2012). The composition of the mesenchymal stromal cell compartment in human bone marrow changes during development and aging. Haematologica *97*, 179–183.

Marwick, J.A., Stevenson, C.S., Giddings, J., MacNee, W., Butler, K., Rahman, I., and Kirkham, P.A. (2006). Cigarette smoke disrupts VEGF165-VEGFR-2 receptor signaling complex in rat lungs and patients with COPD: morphological impact of VEGFR-2 inhibition. Am. J. Physiol. Lung Cell. Mol. Physiol. *290*, L897–L908.

Milpied, P., Massot, B., Renand, A., Diem, S., Herbelin, A., Leite-de-Moraes, M., Rubio, M.T., and Hermine, O. (2011). IL-17-producing invariant NKT cells in lymphoid organs are recent thymic emigrants identified by neuropilin-1 expression. Blood *118*, 2993–3002.

Mjösberg, J., and Spits, H. (2016). Human innate lymphoid cells. J. Allergy Clin. Immunol. *138*, 1265–1276.

Mori, M., Andersson, C.K., Svedberg, K.A., Glader, P., Bergqvist, A., Shikhagaie, M., Löfdahl, C.G., and Erjefält, J.S. (2013). Appearance of remodelled and dendritic cell-rich alveolar-lymphoid interfaces provides a structural basis for increased alveolar antigen uptake in chronic obstructive pulmonary disease. Thorax *68*, 521–531.

Pitzalis, C., Jones, G.W., Bombardieri, M., and Jones, S.A. (2014). Ectopic lymphoid-like structures in infection, cancer and autoimmunity. Nat. Rev. Immunol. *14*, 447–462.

Rabe, K.F., Hurd, S., Anzueto, A., Barnes, P.J., Buist, S.A., Calverley, P., Fukuchi, Y., Jenkins, C., Rodriguez-Roisin, R., van Weel, C., and Zielinski, J.; Global Initiative for Chronic Obstructive Lung Disease (2007). Global strategy for the diagnosis, management, and prevention of chronic obstructive pulmonary disease: GOLD executive summary. Am. J. Respir. Crit. Care Med. *176*, 532–555.

Reference Genome Group of the Gene Ontology Consortium (2009). The Gene Ontology's Reference Genome Project: a unified framework for functional annotation across species. PLoS Comput. Biol. *5*, e1000431.

Roan, F., Stoklasek, T.A., Whalen, E., Molitor, J.A., Bluestone, J.A., Buckner, J.H., and Ziegler, S.F. (2016). CD4+ group 1 innate lymphoid cells (ILC) form a functionally distinct ILC subset that is increased in systemic sclerosis. J. Immunol. *196*, 2051–2062.

Robinette, M.L., Fuchs, A., Cortez, V.S., Lee, J.S., Wang, Y., Durum, S.K., Gilfillan, S., and Colonna, M.; Immunological Genome Consortium (2015). Transcriptional programs define molecular characteristics of innate lymphoid cell classes and subsets. Nat. Immunol. *16*, 306–317.

Roos, A.B., Sandén, C., Mori, M., Bjermer, L., Stampfli, M.R., and Erjefält, J.S. (2015). IL-17A is elevated in end-stage chronic obstructive pulmonary disease and contributes to cigarette smoke-induced lymphoid neogenesis. Am. J. Respir. Crit. Care Med. *191*, 1232–1241.

Scoville, S.D., Mundy-Bosse, B.L., Zhang, M.H., Chen, L., Zhang, X., Keller, K.A., Hughes, T., Chen, L., Cheng, S., Bergin, S.M., et al. (2016). A progenitor cell expressing transcription factor RORγt generates all human innate lymphoid cell subsets. Immunity *44*, 1140–1150.

Silver, J.S., Kearley, J., Copenhaver, A.M., Sanden, C., Mori, M., Yu, L., Pritchard, G.H., Berlin, A.A., Hunter, C.A., Bowler, R., et al. (2016). Inflammatory triggers associated with exacerbations of COPD orchestrate plasticity of group 2 innate lymphoid cells in the lungs. Nat. Immunol. *17*, 626–635.

Subramanian, A., Tamayo, P., Mootha, V.K., Mukherjee, S., Ebert, B.L., Gillette, M.A., Paulovich, A., Pomeroy, S.L., Golub, T.R., Lander, E.S., and Mesirov, J.P. (2005). Gene set enrichment analysis: a knowledge-based approach for interpreting genome-wide expression profiles. Proc. Natl. Acad. Sci. USA *102*, 15545–15550.

Suzuki, T., Hirakawa, S., Shimauchi, T., Ito, T., Sakabe, J., Detmar, M., and Tokura, Y. (2014). VEGF-A promotes IL-17A-producing γδ T cell accumulation in mouse skin and serves as a chemotactic factor for plasmacytoid dendritic cells. J. Dermatol. Sci. *74*, 116–124.

Thorley, A.J., and Tetley, T.D. (2007). Pulmonary epithelium, cigarette smoke, and chronic obstructive pulmonary disease. Int. J. Chron. Obstruct. Pulmon. Dis. *2*, 409–428.

Tschernig, T., and Pabst, R. (2000). Bronchus-associated lymphoid tissue (BALT) is not present in the normal adult lung but in different diseases. Pathobiology *68*, 1–8.

Vacca, P., Montaldo, E., Croxatto, D., Loiacono, F., Canegallo, F., Venturini, P.L., Moretta, L., and Mingari, M.C. (2015). Identification of diverse innate lymphoid cells in human decidua. Mucosal Immunol. *8*, 254–264.

Van Pottelberge, G.R., Bracke, K.R., Van den Broeck, S., Reinartz, S.M., van Drunen, C.M., Wouters, E.F., Verleden, G.M., Vermassen, F.E., Joos, G.F., and Brusselle, G.G. (2010). Plasmacytoid dendritic cells in pulmonary lymphoid follicles of patients with COPD. Eur. Respir. J. *36*, 781–791.

Yadav, M., Louvet, C., Davini, D., Gardner, J.M., Martinez-Llordella, M., Bailey-Bucktrout, S., Anthony, B.A., Sverdrup, F.M., Head, R., Kuster, D.J., et al. (2012). Neuropilin-1 distinguishes natural and inducible regulatory T cells among regulatory T cell subsets in vivo. J. Exp. Med. *209*, 1713–1722, S1–S19.

Yang, Y.C., Zhang, N., Van Crombruggen, K., Hu, G.H., Hong, S.L., and Bachert, C. (2012). Transforming growth factor-beta1 in inflammatory airway disease: a key for understanding inflammation and remodeling. Allergy *67*, 1193–1202.

Cell Reports, Volume *18*

Supplemental Information

Neuropilin-1 Is Expressed on Lymphoid Tissue Residing LTi-like Group 3 Innate Lymphoid Cells and Associated with Ectopic Lymphoid Aggregates

Medya Mara Shikhagaie, Åsa K. Björklund, Jenny Mjösberg, Jonas S. Erjefält, Anne S. Cornelissen, Xavier Romero Ros, Suzanne M. Bal, Jasper J. Koning, Reina E. Mebius, Michiko Mori, Melanie Bruchard, Bianca Blom, and Hergen Spits

Supplementary Figure 1 related to Figure 1

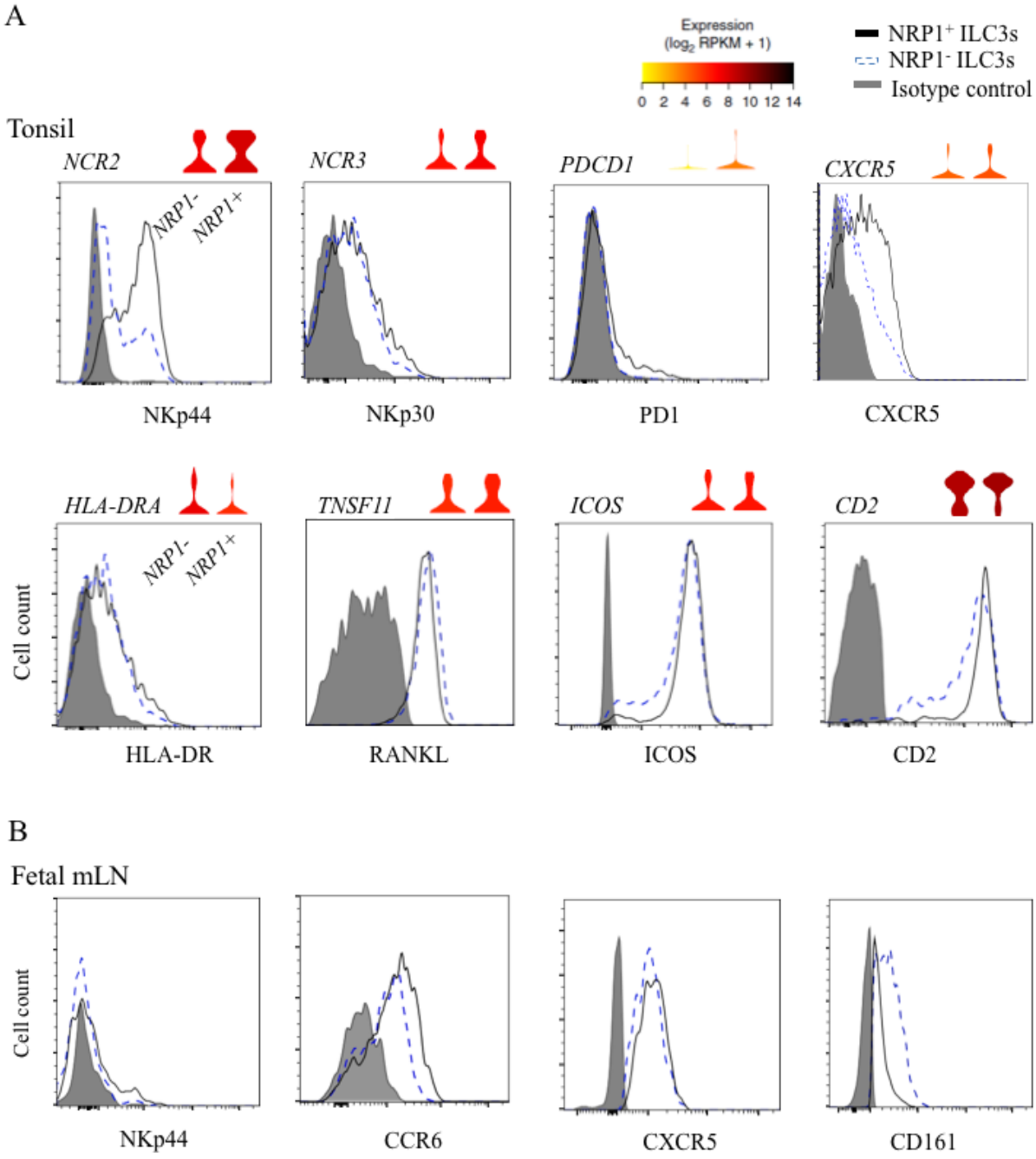

Supplementary Figure 1. A) ILC3s are characterized as lineage negative, CD45 high, CD127 high, CD161 high, CD117 high lymphocytes. Filled histogram shows isotype-matched control antibody. Representative FACS plots showing the expression of surface markers NKp44, PD1, NKp30, HLA-DR, RANKL, ICOS and CD2 on ILC3s. Black open histogram shows $NRP1^+$ ILC3 and dark blue dashed line indicates $NRP1^-$ ILC3. Violin plots

in the upper right corner show, with colour according to mean expression value, the gene expression distribution in *NRP1*$^{+}$ and *NRP1*$^{-}$ ILC3 as determined by scRNA-seq (5). **B)** Representative FACS plots showing the expression of CCR6 expression, NKp44, CXCR5 and CD161 on fetal mLN ILC3. Black open histogram shows NRP1^{+} ILC3 and dark blue dashed line indicating NRP1^{-} ILC3. Grey histogram indicates staining with isotype-matched control antibody.

Supplementary Figure 2 related to Figure 4

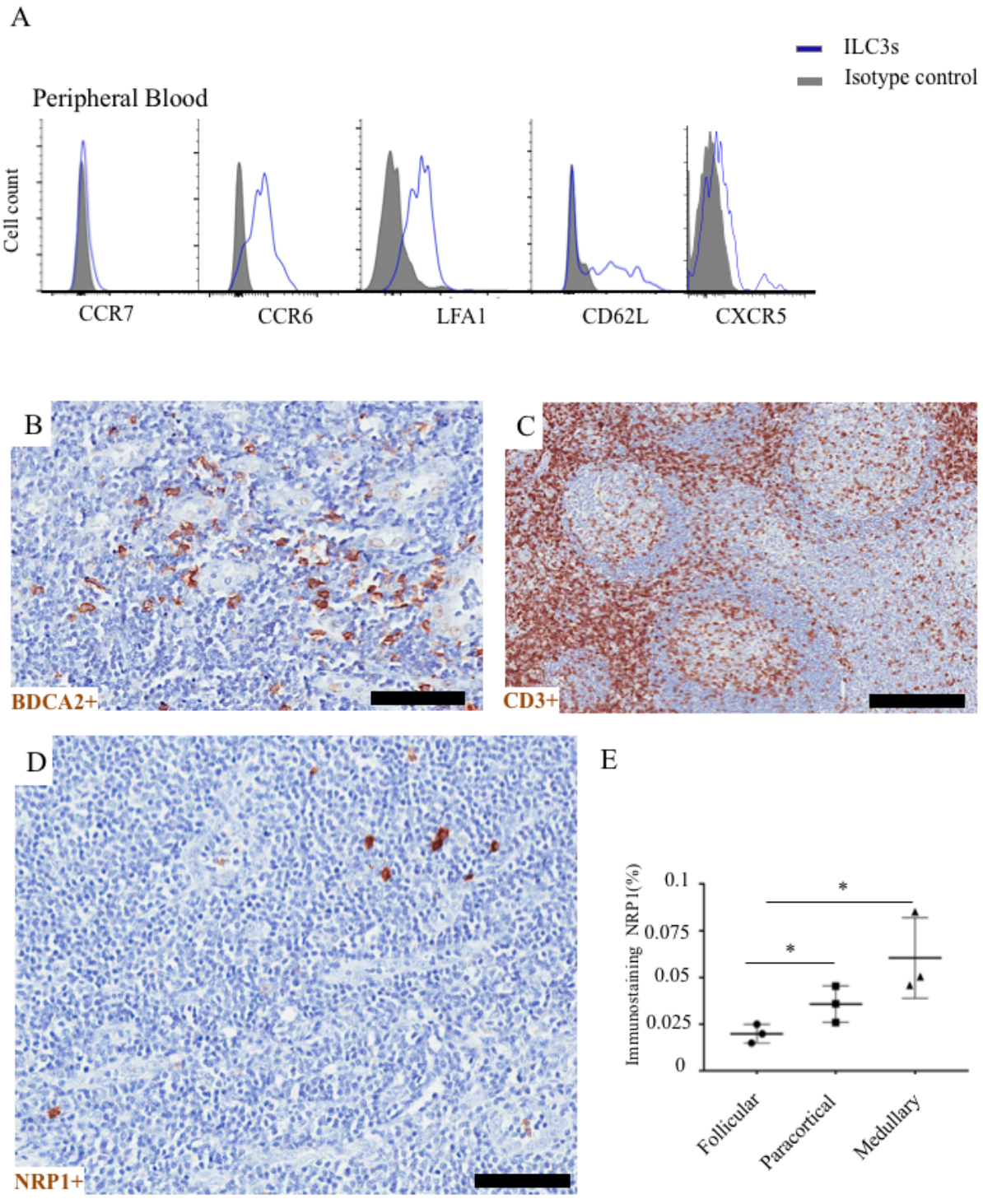

Supplementary Figure 2. A) Cell surface expression of CCR7, CCR6, LFA1, CD62L, CXCR5 and NRP1 on freshly isolated ILC3 from peripheral blood (dark blue line) assessed

by flow cytometry. Filled histogram shows isotype control. **B)** Photomicrograph showing single IHC stains (*brown stain*) of CD3, BDCA2 and NRP1. Sections are counterstained with Mayer's hematoxylin (*blue stain*). Experiments with 3 donor tissues showed similar results. Black scale bar = 100 μm.

Supplementary Figure 3 related to Figure 5

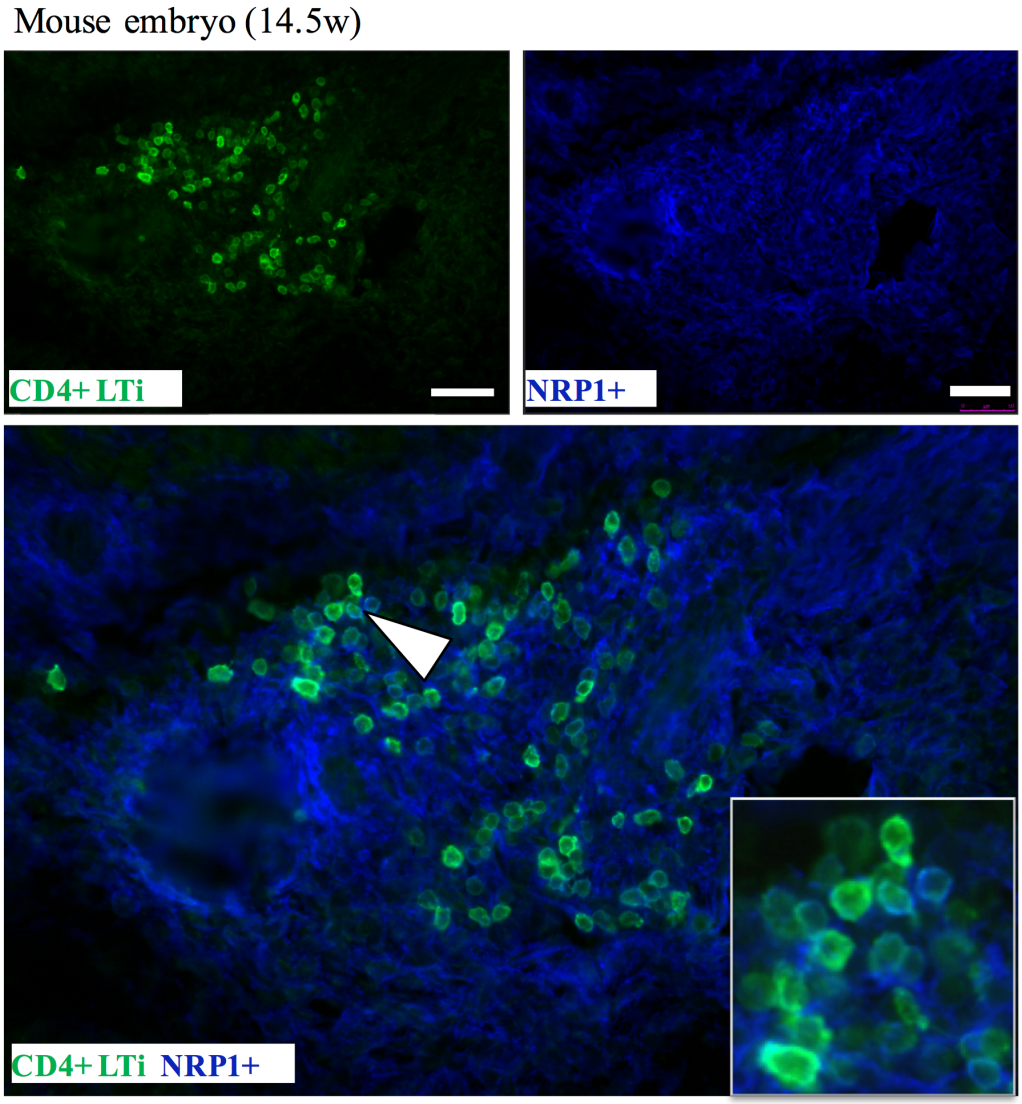

Supplementary Figure 3. Photomicrograph showing IHC stained sections from E14.5 mouse embryo. $CD4^+$ LTi cells (*green stain*) and NRP1 (*blue stain*). White scale bar = 100 µm.

Supplementary Figure 4 related to Figure 7

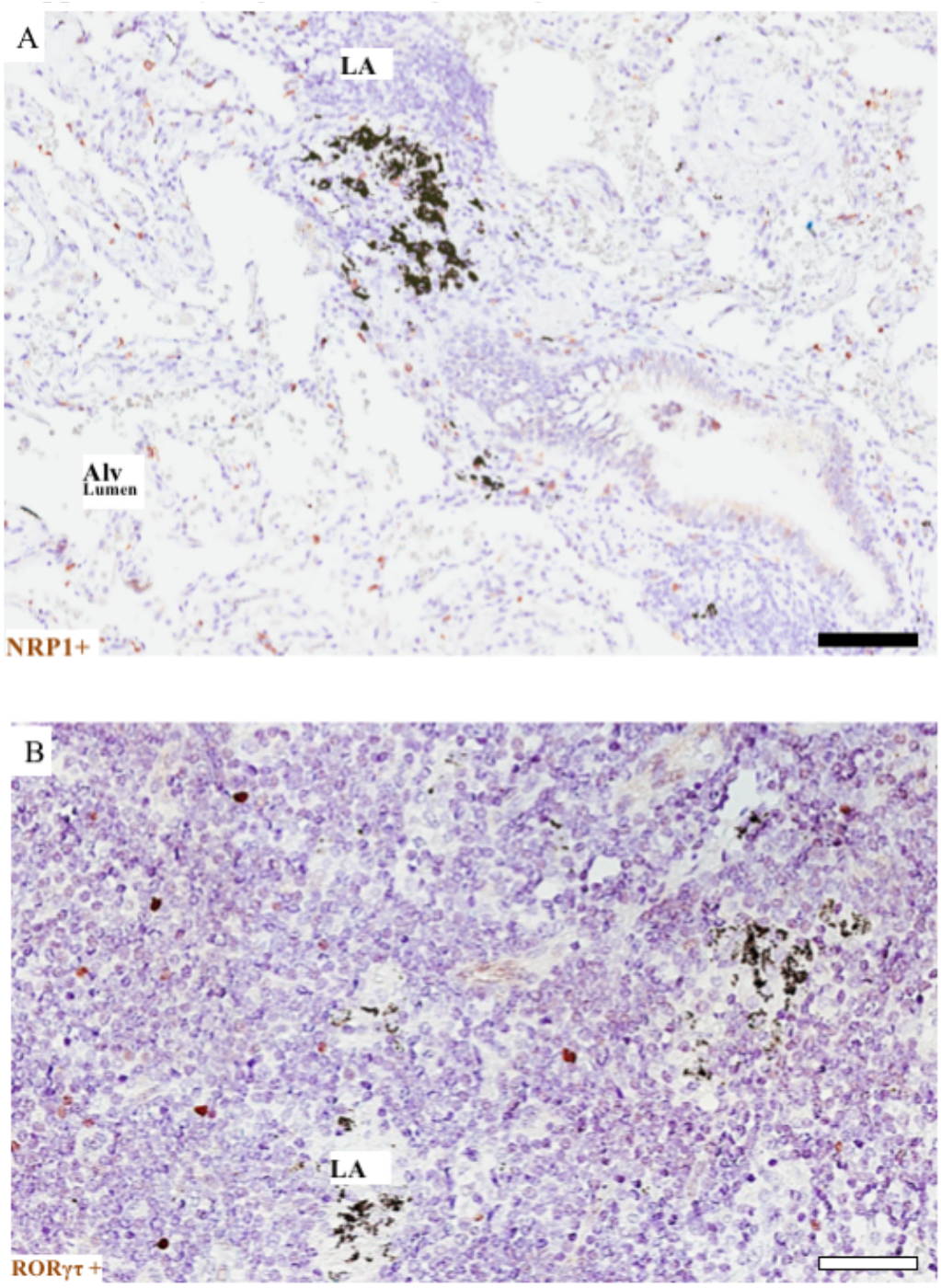

Supplementary Figure 4. Photomicrograph showing single IHC stains (*brown stain*) of **A)** $NRP1^{+}$ cells in peripheral lung tissue, including alveolar (Alv) lumen and lymphoid aggregates (LA). **B)** RORγτ staining in LA from COPD patients. All sections were counterstained with Meyer hematoxilin. Black endogenous pigments are visible. Black scale bar = 100 μm; white scale bar = 50 μm.